Interdiffusion in the polycrystalline systems Er_2O_3-Y_2O_3 and Er_2O_3-H_2O_3

by

Gregory Raymond Gessel

A Thesis Submitted to the
Graduate Faculty in Partial Fulfillment of
The Requirements for the Degree of
MASTER OF SCIENCE

Major Subject: Nuclear Engineering

Iowa State University
Ames, Iowa

1971

TABLE OF CONTENTS

	Page
INTRODUCTION	1
LITERATURE REVIEW	5
Diffusion in General	5
Diffusion in Rare-Earth Oxides	7
THEORY	9
Continuum Approach to Diffusion	9
Atomistic Approach to Diffusion	12
Particular Mechanisms of Diffusion	16
PROCEDURE	19
Fundamental Considerations	19
Materials, Techniques and Equipment	23
Additional Investigations Relating to Specimen Preparation	31
RESULTS AND DISCUSSION	39
CONCLUSIONS	77
SUGGESTIONS FOR FURTHER WORK	78
BIBLIOGRAPHY	80
ACKNOWLEDGMENTS	84
APPENDIX	85
Modifications of Fick's Laws	85

INTRODUCTION

During the past two decades many developments in nuclear technology have been seen and perhaps most significant has been the advent of commercial use of nuclear energy. The assumption of this role has brought nuclear technology into the struggle for higher efficiencies as a consequence of the desire to give consumers the lowest cost per unit of energy. This efficiency problem is by no means new, but rather has occupied the fossil fuel plant designers for years. Although several methods to increase efficiency have been proposed and examined, the general trend has been in the direction of increasing reactor operating temperatures, which has the effect of providing a greater Carnot efficiency. However, this type of solution will impose increasingly stringent requirements on reactor materials which already are forced to operate in a hostile environment. As a result, reactor development has been closely linked to material science. As operating temperatures go up, the list of materials capable of meeting temperature requirements alone diminishes. Certain refractory oxides and carbides have good high temperature stability and thus UC, UO_2, PuC and PuO_2 have developed as nuclear fuels. Certainly as important as the fuel to be fissioned is the control material needed to regulate the process. It would appear that refractory oxides could also be considered for this job as well. It is for this role that the rare-earth oxides,

considered in this study, may be suited.

The requirements that such a control material would need to satisfy should be reviewed. At the outset a control material must be capable of withstanding both a high temperature and a high radiation environment. In order to afford good control, thermal reactors require absorbers with thermal neutron absorption cross sections (σ_a^{th}) near 100 barns. However, the Σ_a^{th} should not be so high as to make the control element black to neutrons. The reasoning here is that black control rods greatly distort the flux and cause undesirable temperature distributions. Current use of materials such as hafnium (σ_a = 100 barns) has been due to these considerations. While hafnium can exist as a refractory oxide, it requires stabilization. There is a strong possibility that in a high radiation environment hafnia would destabilize resulting in undesirable physical distortion.

On the other hand, the rare earth oxides Ho_2O_3, Y_2O_3 and Er_2O_3 seem well suited for use as control elements. Absorption cross sections are 65b for Ho, 1.28b for Y and 106b for Er. In addition these rare-earths show substantial epithermal resonances. The effective cross section of a Er_2O_3 control element could be reduced by addition of either Y_2O_3 or Ho_2O_3. Within the temperature range one would consider for reactor operation these oxides do not require stabilization. In fact the first phase changes observed in the oxides Ho_2O_3, Y_2O_3 and

Er_2O_3 occur above 2200°C [1].

Information about the diffusion phenomenon is of great importance in reactor materials considerations. This is due to the exponential temperature dependence of diffusion and also to the material property changes that can result from diffusion. With the similarity of physical properties of Y_2O_3, Ho_2O_3 and Er_2O_3 it could however be argued that diffusion would result in only minor changes. Perhaps more important is the role that a study of interdiffusion in these materials may play in shedding more light on the diffusion process itself. Berard [2] for example found an unexpected variation in activation energy for self diffusion in Y_2O_3 and Er_2O_3. Because of the similarities of the Y and Er ions, the observed variation could not be explained. In fact the only significant difference between the ions is that they differ by a factor of two in mass. The possibility that the variation in activation energy is mass dependent forms the basis for this investigation. In order to maximize any possible mass effects, interdiffusion in the systems Y_2O_3-Er_2O_3 and Ho_2O_3-Er_2O_3 was studied. The significant point about these systems is that in the first a maximum mass difference exists while a minimum exists for the second system. The rare-earths seem particularly well suited for this type of study since their physical and chemical properties are nearly identical.

Thus, with the intent of providing information which

will help permit a true evaluation of the application of rare earth oxides for nuclear reactor control, this investigation has the following objectives.

1. To obtain interdiffusion coefficients in the systems Er_2O_3-Y_2O_3 and Er_2O_3-Ho_2O_3.
2. To obtain Arrhenius plots from which the influence of ion mass on interdiffusion can be inferred.

It is this author's belief that at the present time a Y_2O_3-Er_2O_3 or Ho_2O_3-Er_2O_3 control element is prohibited only by cost. Ames Laboratory represents one of a few producers of ultra-high purity (99.99%) rare-earths; however commercial concerns have started to produce high purity rare earths. It is entirely possible that this high degree of purity would not necessarily be required of a control material. Careful consideration would need to be given to such items as compatibility and effects of impurities on rod physical properties. With the needed physical parameters at hand and competitive prices available, reactor designers could then incorporate the advantages of the rare-earth oxides in an effort to achieve still higher operating temperatures and greater thermal cycle efficiencies. For these reasons, it is conceivable that the rare-earth oxides, Y_2O_3, Ho_2O_3 and Er_2O_3 merit consideration as control materials in for example a high temperature gas cooled reactor concept.

LITERATURE REVIEW

Diffusion in General

Since the mid-19th century, when the first quantitative diffusion work was being done, diffusion literature has grown at an ever increasing rate. Several bibliographies have appeared in an effort to consolidate the available literature. One such listing [3] covers diffusion of gases, liquids and solids in solids in the period 1890 to 1955. Berard [4] has treated ceramic systems while oxides have been covered by Lommel [5], Linder [6], Cumming and Harrop [7], Askill [8] and Alper [9]. Also available is a periodical, Diffusion Data [10], which has as its sole purpose the compilation of diffusion work.

Crank [11] has treated extensively the mathematics of the process while Jost [12] examined diffusion in general. Frank-Kamenetskii [13] has treated diffusion in chemical kinetics.

More specifically, several authors have chosen to consider only the diffusion phenomenon in solid state. Barrer [14] and Shewmon [15] have considered diffusion in solids in general. Girifalco [16] has treated the subject for the layman. Perhaps one of the most comprehensive treatments of solid state diffusion has been given by Adda and Philibert [17]. American Society for Metals [18,19], Mehl [20], Andelin and Godfrey [21] and Svechnikov [22] have been concerned with diffusion in metals only. Diffusion in ionic solids has been examined by

Giess [23], Suptitz and Teltow [24], Herman [25] and Birchenall [26].

From time to time symposia have dealt with diffusion [27] and more specifically diffusion in oxides [28].

Over the years several methods have been developed to measure diffusion coefficients. Berard [29] has examined the methods and their historic development. One interesting and unique method combined activation analysis and sectioning [30, 31]. The question of what happens to an already established penetration profile when it is subjected to neutron activation has also been considered [32,33]. Recently the electron microprobe has been established as an important tool for diffusion profile analysis [34].

More directly related to the nuclear materials field, diffusion in various uranium reactor fuels has been reviewed by Walter [35]. Current work in cladding and reactor structure materials has been treated by Ashurst [36].

After reading much of the available literature on diffusion one is impressed by a number of points. "Diffusion" has been around a long time, however it is far from totally understood. This is probably due to the fact that it is often related to, and affected by, many material properties. This statement characterizes the materials science which is a field characterized by too many variables interrelated in unknown ways. Much of the solid state diffusion work has been done

on metals leaving ceramics all but untouched. This has of course been changing as demands are placed on materials that can be best met by ceramics. So, in general, diffusion is a field of study that has developed and can look forward to further development.

Diffusion in Rare-Earth Oxides

At present very little diffusion data in rare-earth oxides has been compiled. To the knowledge of this author, the study of interdiffusion in rare-earth oxides has not been attempted. With respect to diffusion processes in polycrystalline rare-earth oxides, Berard [2] studied both cation self diffusion and oxygen diffusion in Y_2O_3 and Er_2O_3. Berard *et al.*[37] have used a thermobalance technique to study oxygen transport in Sc_2O_3, Y_2O_3, Dy_2O_3, Ho_2O_3, Er_2O_3, Tm_2O_3 and Lu_2O_3. Diffusion of oxygen in rare-earth oxides has also been treated by Minachev and Antoshin but the materials were impure [38]. Other studies of oxygen transport in rare-earth oxides include Sazonov *et al.* [39] on Nd_2O_3, Stone [40] on Eu_2O_3, Nd_2O_3 and Sm_2O_3, Vinokurov [41] on CeO_2, Wirkus *et al.* [42] on Gd_2O_3, and Svec and Rider [43] on Tm_2O_3.

Properties of the lanthanides of which Y, Er and Ho are examples, are in general not well known and a considerable portion of continuing work is being conducted at Ames Laboratory of the AEC. The proximity of both material and special-

ized expertise in this field has aided this project greatly. As evidence for the pertinence of this study, a few commercial industrial firms have become involved in the production of rare earth metals and compounds.

THEORY

Continuum Approach to Diffusion

Diffusion processes represent a part of a much larger class of problems generally termed transport phenomena. When molecular processes are ignored and the continuum approach is undertaken, similarities in the treatment of energy, momentum and mass transport appear. This fact allowed Fick [44] in 1855 to draw on a development of Fourier [45] for heat conduction and develop the first consistent set of equations governing diffusion. Strictly speaking, Fick treated an isothermal, isobaric, one dimensional, binary gaseous system. However, with little effort one can extend this treatment to accommodate more general situations. For example, situations of interest might include multidimensional diffusion. The precise form of the media, whether gas, liquid or solid, is irrelevant since it is ultimately treated as a continuum. Extended versions of the diffusion equations will be presented here.

Fick's first equation in modified form is.

$$J_i = -D_{ij} C_{,j} \tag{1}$$

The Cartesian tensor notation has been used. The underlying principle involved in this equation is the proportionality between the flux J_i and the concentration gradient $C_{,j}$ through a diffusion tensor D_{ij}. Fick's first law is best regarded as a definition of the diffusion tensor.

The second law of Fick treats the nonsteady state system and is

$$\dot{C} = (D_{ij}\, C_{,j})_{,j} \tag{2}$$

This equation can be generated by performing a material balance on a unit volume of the medium. By assuming conservation of matter and Equation 1, one obtains Equation 2.

In actuality, Fick's treatment of diffusion is misleading in that it suggests that the driving force for a flux is a gradient in concentration. Darken in [19] has argued that a gradient in chemical potential is a more likely driving force for diffusion. This is not to say that Fick's equations are inaccurate but rather that they can be put in more readily interpretable form. Suitable rearrangement, described in the Appendix, yields the following expressions for Equations 1 and 2.

$$J_i = -B_{ij}\, C\, \mu_{,j} \tag{3}$$

$$C = (B_{ij}\, C\, \mu_{,j})_{,j} \tag{4}$$

Here B_{ij} is the mobility, C is the concentration and $\mu_{,j}$ is the gradient in chemical potential.

During the interdiffusion of different species, the phenomenon treated in this study, the result is a series of solid solutions, provided that no compounds form. This type of situation plus the possibility of nonideal mixing of the

species calls for a further alteration of both Fick's and Darken's equations. Again the necessary manipulations are relatively simple and are presented in the Appendix. The results are

$$J_i = (-D_{ij}[1 + \frac{\partial \log \gamma}{\partial \log N}] C_{,j})_{,j} \quad (5)$$

$$\dot{C} = (D_{ij}[1 + \frac{\partial \log \gamma}{\partial \log N}] C_{,j})_{,j} \quad (6)$$

Where γ is the activity coefficient and N represents the mole fraction. By comparison with Equations 3 and 4 the appearance of a thermodynamic correction factor is noted. Thus the most general case of nonideal solutions can be treated within the framework of Fick's equations. For an ideal solution, the $[1 + \partial \log \gamma / \partial \log N]$ term reduces to unity and Equations 5 and 6 become Fick's first and second laws respectively.

Fick's laws, coupled with the appropriate boundary conditions, can be used to obtain concentration as a function of time and position. There are however important limiting situations which cannot be adequately described by Fick's laws. These cases include systems in which additional driving forces are present. This separate class of problems will not be treated here, but can be handled with additional terms in the appropriate diffusion equations.

Atomistic Approach to Diffusion

As previously stated, a continuum approach completely ignores any molecular processes. Intuitively, the elimination of a chemical potential gradient by mass transport must ultimately involve atomistic movement through the matrix. Atomistic considerations open a whole new area concerned with mechanisms by which atoms move in solids. Relatively speaking, solids are ordered structures implying that only certain paths of movement are energetically favored. Consequently, the structure of the solid is a major factor influencing the types of movement-mechanisms possible. In general, a mechanism offering the lowest energy configuration is favored. For purposes of this discussion only those mechanisms which involve movement of thermally created defects will be considered.

Diffusion can then be treated as a random walk process whereby an atom proceeds through a solid by jumping from one vacant lattice site to another. Clearly, the jump rate governs the process. Jump rate can be treated as the product of three terms, the probability of a given adjacent site being vacant, the rate of attempted jumps of the atom into a given adjacent site, and the number of adjacent sites n.

At thermal equilibrium, the probability of an adjacent site being vacant is, according to Boltzman statistics

$$P = \exp - \left(\frac{\Delta G_f}{kT} \right), \qquad (7)$$

where ΔG_f is the free energy of formation of the vacancy and k and T have their usual meanings.

Since energy is required to move from one site to another, the rate of jump attempts toward a specific vacant site is

$$\omega = \upsilon_o n \exp - \left(\frac{\Delta G_m}{kT} \right) \tag{8}$$

Where ω is the rate of jump attempts toward a specific vacant site, υ_o is the vibration rate toward a specific vacant site and ΔG_m is the free energy of movement. The exp $- (\Delta G_m/kT)$ term can be viewed as the probability that a given oscillation will have sufficient energy to achieve a saddlepoint configuration.

Combining these terms one obtains an expression for the jump frequency Γ of the form

$$\Gamma = \upsilon_o \exp \left(\frac{\Delta S_f + \Delta S_m}{k} \right) \exp - \left(\frac{\Delta H_m + \Delta H_f}{kT} \right) \tag{9}$$

where the free energies have been decomposed into enthalpy and entropy terms.

On the basis of random walk analysis, (not to be treated here) the diffusion coefficient can be defined as

$$D = \frac{1}{6} \alpha^2 n \omega p \tag{10}$$

where α is the jump distance and n, ω and p have been previously defined. By introducing the lattice parameter a_o and

defining $\gamma = n\alpha^2/6a_o^2$ one obtains for the diffusion coefficient

$$D = \gamma a_o^2 \omega p \tag{11}$$

By substitution it can be seen that

$$D = \gamma a_o^2 \upsilon_o \exp\left(\frac{\Delta S_f + \Delta S_m}{k}\right) \exp -\left(\frac{\Delta H_f + \Delta H_m}{kT}\right) \tag{12}$$

It should be noted that the development of Equation 12 assumed a random walk process.

Important situations arise when atom movements are not random but correlated. In these cases a correlation coefficient $f(\leq 1)$ must be included in Equation 12.

Determination of f involves summing the number of nearest neighbor sites into which an atom can migrate after X jumps. The calculation of f can be a tedious matter and good estimates require the assistance of a computer. Several authors have considered correlation effects and a classic in this area is the paper of Barr and LeClaire [46].

Experimentally, the diffusion coefficient is usually found to fit an Arrhenius relation of the form

$$D = D_o \exp -\left(\frac{Q}{kT}\right) \tag{13}$$

where D_o and Q are independent of temperature. The Q term has been generally called the activation energy. The term activation energy resulted from picturing an atom moving from one lattice site to another as going through a potential

energy barrier.

Comparison of Equation 12 with Equation 13 leads one to equate the similar terms.

$$D_o = \gamma a_o^2 \upsilon_o \exp\left(\frac{\Delta S_m + \Delta S_f}{k} \right) \tag{14}$$

and

$$Q = \Delta H_f + \Delta H_m \tag{15}$$

The atomistic approach developed as a result of attempts to explain the Arrhenius form of the data. The form of these expressions is largely the result of work by Zener [47] and Wert [48]. Attempts to explain the form of Equation 13 have been made by Glasstone, Laidier and Eyring [49] using absolute rate theory; however this approach has been becoming less popular. The most recent treatments involve consideration of the vibrational modes available to the atom constrained by the lattice.

The most rigorous treatment of the problem involves considering all the various degrees of freedom available to the jumping atom. Treatments have typically been greatly simplified by constraining the atom to vibrations along only one axis. The problem is complicated and must ultimately involve many body considerations as the effects of neighboring atoms need to be considered.

Particular Mechanisms of Diffusion

Several diffusion jump mechanisms have been considered and treated by Manning [50], Zener [51], Shewmon [15] and others. On the basis of the cubic c-type rare-earth oxide structure, which Ho_2O_3, Er_2O_3 and Y_2O_3 have been shown to display [52], one can argue that diffusion of the cation species will most likely proceed by a vacancy mechanism. The argument is basically that, at the temperatures of interest the potential barrier presented to the cation trying to jump by any other mechanism is likely to be too great. The vacancy mechanism has been treated in great detail elsewhere [24,53].

In actual diffusion experiments other mechanisms must either be considered or efforts must be made to eliminate their effects. Specifically in polycrystalline solids, grain boundary diffusion must be considered, while in all solid state diffusion experiments, steps must be taken to reduce surface diffusion.

In polycrystalline solids, the region of disorder which bounds the individual crystallites or grains is termed the grain boundary. The grain boundary is said to contain diffusion pipes since mass transport may proceed several orders of magnitude more rapidly in the grain boundary than in the crystallites. Thus grain boundaries enhance the bulk diffusion in polycrystalline solids. The degree of enhancement in a cross section will be proportional to the ratio of

the grain boundary area to the grain area. Mathematical models have been advanced by Fisher [54], Whipple [55] and Suzuoka [56]. Canon and Stark [57] compared these three models by examining results from computational solutions of each. A number of other papers have appeared which treat the grain boundary problem; some more recent ones include [58,59, 60]. Wvensch and Vasilos [61] and Austin and Richard [62] have used the electron microprobe to analyze the diffusion of material along grain boundaries.

Relative to diffusion in the matrix, diffusion along surfaces is also probably considerably more rapid. Thus an effort was made to obtain solids for diffusion studies which were as near theoretical density as possible. Densities less than theoretical imply the presence of internal voids. These voids can be either pores or cracks but nevertheless represent internal surfaces. The net effect of such internal surfaces is the enhancement of bulk diffusion and has been considered by Mortlock [63]. In referring to surface diffusion a surface diffusion coefficient D_s is used. Surface diffusion has interested several investigators due to the unexplained behavior of the ln D_s vs. 1/T plot. The observed change in slope of the Arrhenius plot has been explained as indicating a change of mechanism [64]. An explanation involves postulating both vacancy and adatom surface diffusion mechanisms which predominate over different temperature ranges. D_s the

surface diffusion coefficient can be expressed as

$$D_s = D_o^v \exp -\left[\frac{\Delta H_f^v + \Delta H_m^v}{kT} \right] + D_o^a \exp -\left[\frac{\Delta H_f^a + \Delta H_m^a}{kT} \right] \qquad (16)$$

where superscript v refers to vacancy, superscript a refers to adatom,

$$D_o^v = \gamma a_v^2 \nu_v \exp\left[\frac{\Delta S_f + \Delta S_m}{k} \right] \text{ and } D_o^a = \gamma a_a^2 \nu_a \exp\left[\frac{\Delta S_f + \Delta S_m}{k} \right].$$

Here it should be noted that a_v^2 and a_a^2 are no longer restricted to the value of one lattice parameter. With D_s viewed as the sum of both D^v and D^a the problem of explaining the high D_o term experimentally observed at high temperatures, turns out to be no easy matter. Although several explanations have been advanced [65,66,67], none seem to satisfactorily explain the observed change in slope of the Arrhenius plot.

PROCEDURE

Fundamental Considerations

It will be recalled that the objective of this study is to determine the interdiffusion coefficients of the systems Y_2O_3-Er_2O_3 and Ho_2O_3-Er_2O_3 over a temperature range. Experimentally this involves placing two slabs of pure material in intimate contact and allowing the species to interdiffuse. Although simple in principle, experimentally the matter is complicated and consideration must be given to maintaining certain boundary conditions so that solutions can be obtained to the Fick's laws equations.

In order to allow for meaningful data reduction and interpretation, the limiting situation of one-dimensional geometry was chosen. With this simplification Equations 1 and 2 become

$$J_X = - \tilde{D} \frac{\partial C}{\partial X} \tag{17}$$

$$\frac{\partial C}{\partial t} = \frac{\partial}{\partial X} \tilde{D} \frac{\partial C}{\partial X} \tag{18}$$

where $\tilde{D}$ is the interdiffusion coefficient. In a binary system the following interface conditions apply.

$$J_A = -J_B \tag{19}$$

$$\frac{\partial C_A}{\partial X} = - \frac{\partial C_B}{\partial X} \tag{20}$$

Here the interdiffusing species are A and B. Initial conditions, for this problem, require that at time t = 0 pure A be present on one side of the interface and pure B on the other. In addition, it is required that each side be much greater in extent than the diffusion zone. Equations 17 and 18 coupled with 19 and 20 and the initial and boundary conditions given above are commonly referred to as the "inexhaustible-semi-infinite case".

It goes without saying that the experiment must conform to the assumed mathematical description if valid results are to be obtained using the given equations. It turns out that both the interface condition and the one dimensional simplification require that careful consideration be given to achieving and maintaining good contact between the diffusion couples. Reference to Figure 1, which shows, schematically, a poor contact situation, will help in understanding this requirement.

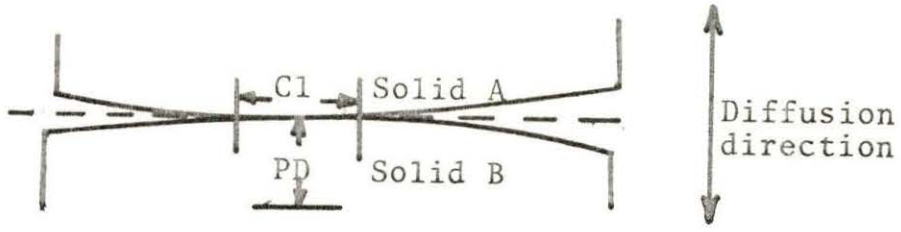

Figure 1. Diffusion couple showing effect of poor contact

Intuitively, one would guess that when contact line Cl is of the order of the penetration depth PD, and certainly when it is less, two-dimensional diffusion will occur. As will be seen later, careful consideration was given to obtaining and maintaining good contact between the two diffusion couples, i.e. Cl >> PD.

In general the $\tilde{D}$ term is found to be concentration dependent, thus Equation 18 is nonhomogeneous. Because of the difficulty of obtaining an analytical solution to 18, special methods have been developed which incorporate graphical techniques. One such method is the Boltzmann-Matano method [68]. Basically this technique involves transforming Equation 18 into a homogeneous form. The end result of this analysis (provided in any text on diffusion Reference (11)) os

$$\tilde{D}(C_1) = - \frac{1}{2t}\left(\frac{dX}{dC}\right)\Big|_{C_1} \int_o^{C_1} X \, dC \qquad (21)$$

where $\tilde{D}(C_1)$ is the interdiffusion coefficient at a specific concentration C_1. Graphical determination of $\tilde{D}(C_1)$ involves measuring the slope (dX/dC) at C_1 and the area under the diffusion profile from a Matano interface where X = 0 to C_1. The Boltzmann-Matano method requires the location of a Matano interface which will have an associated uncertainty. It also should be noted that this method does not allow for changes of molar volume upon mixing of the species. A second and more recently developed method is due to Wagner [69]. The

Wagner method is somewhat similar to the Boltzmann-Matano method with the notable exception that variations of molar volume are treated. A Matano interface is not required, however. In the rare-earth systems being studied the variation of molar volume is slight, however many systems can be more adequately treated using the more general Wagner method. The Wagner method will not be derived in detail here, however the final result is provided for reference.

$$\tilde{D}(N_2^*) = \frac{(N_2^+ - N_2^-)V_m(N_2^*)}{2t(\partial N_2/\partial X)_{X=X^*}} \left[(1-Y^*)\int_{-\infty}^{X^*} \frac{Y}{V_m}\,dX + Y^*\int_{X^*}^{+\infty} \frac{(1-Y)}{V_m}\,dX\right] \quad (22)$$

where $Y = \dfrac{N_2 - N_2^-}{N_2^+ - N_2^-}$

The notation used in this equation can be understood by reference to Figure 2.

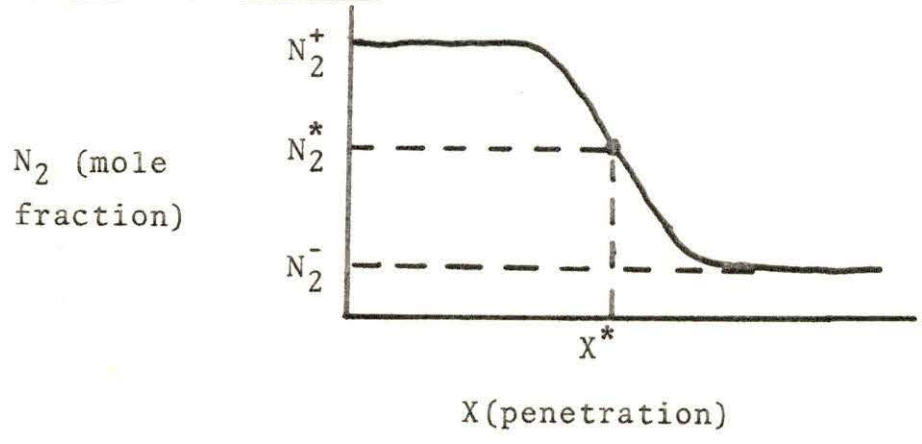

Figure 2. Penetration profile for Wagner method

On the basis of the fact that diffusion data obtained by both methods by the present author, and for the materials of concern, were found to be in good agreement, the decision was made to use the somewhat simpler Matano procedure.

Materials, Techniques and Equipment

Starting materials for this study were provided by the Ames Laboratory in the form of oxides derived from calcination of the oxalates. These "as received" oxides were dissolved in boiling hydrochloric acid and reprecipitated with ammonium hydroxide. The resulting gelatinous precipitate was washed with distilled water, until tests with silver nitrate indicated the absence of the chloride ion, and then dried in an oven at 135°F.

The resultant hydroxides were crushed in a mortar and pestle and calcined at 1200°C. An active powder was produced by removing the calcine from the furnace at 600°C. Individual pellets 1/8 inch thick were cold pressed to 2000 psi in a 3/8 inch carbide lined die using a Carver laboratory press, and then isostatically pressed to 50,000 psi .

The isostatically pressed pellets were then sintered at 1920°C for a period of 2 hours in argon. The furnace used for the sintering operation was a Centorr, see Figure 5. The heating cycle involved a 20 minute rise to 1400°C, a 15 minute hold at 1400°C to allow for outgassing, a 20 minute rise to

1900°C, a 2 hour hold at 1900°C and finally a 45 minute cooling time.

Pellets prepared by this technique were found to have densities consistently above 97% of the X-ray value. Photomicrographs of the sintered Ho_2O_3, Y_2O_3 and Er_2O_3 are shown in Figures 3a, 3b, 3c respectively. The grain size was measured by the Fullman method and found to be 60.29μ for Ho_2O_3, 55.11μ for Y_2O_3 and 41.58μ for Er_2O_3.

In order to delineate adequately the grain boundaries a 2 minute etch with hot H_2SO_4 was required. Because of the long etch time required, all these photomicrographs show an abundance of etch pits. These should not be confused with porosity. It should be noted that pores are generally circular while etch pits appear rectangular. Unetched specimens showed that most of the porosity present in the sintered specimens was confined to the grain boundaries. The etch pits appear to be intragranular.

Sintered specimens were subjected to emission spectrographic analysis and found to be as pure as the starting material. Table 1 presents the results of this quantitative analysis.

In low oxygen partial pressure environments at elevated temperatures the rare-earth oxides have a tendency to lose oxygen and assume a nonstoichiometric composition. Since in this study stoichiometry was not to be a variable, it was

Figure 3. Photomicrographs of isostatically pressed and sintered rare earth oxides

A. (top) Etched Ho_2O_3 specimen; magnification 160X

B. (middle) Etched Y_2O_3 specimen; magnification 160X

C. (bottom) Etched Er_2O_3 specimen; magnification 160X

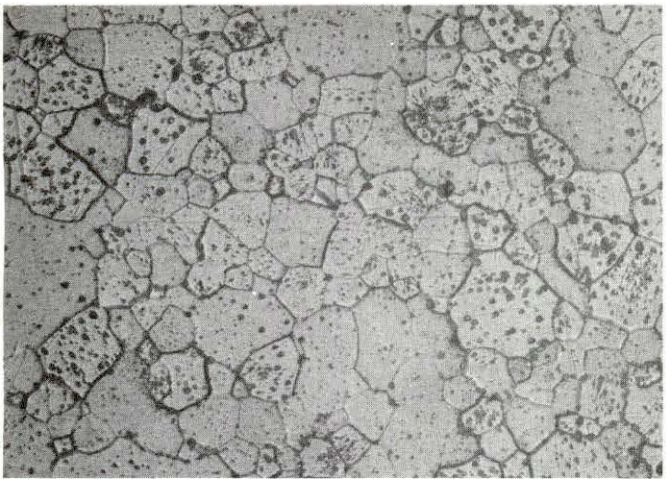

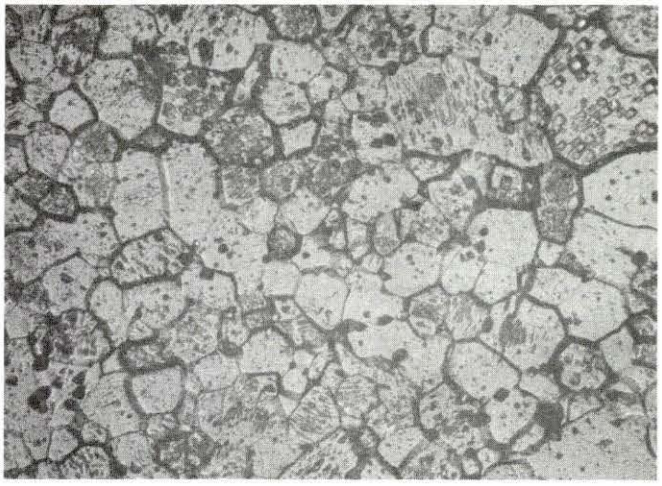

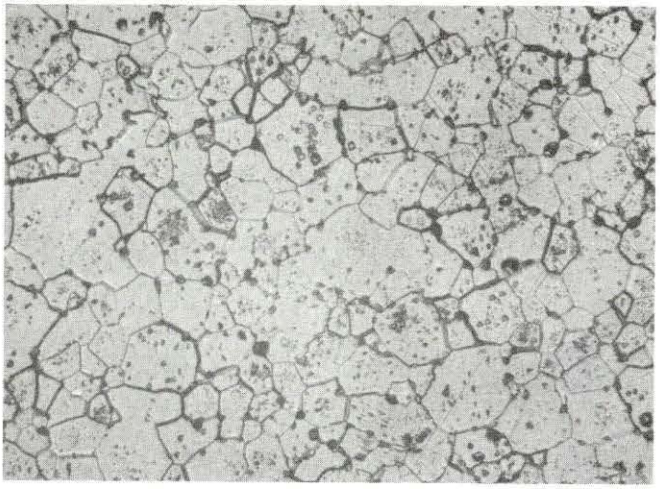

Table 1. Emission spectrographic analysis of the sintered oxides (ppm)

Element	Y_2O_3	Ho_2O_3	Er_2O_3
Ce	N.D.[a]	N.D.	N.D.
Pr	N.D.	N.D.	N.D.
Nd	N.D.	N.D.	N.D.
Sm	N.D.	N.D.	N.D.
Eu	<20	N.D.	N.D.
Gd	N.D.	N.D.	N.D.
Tb	N.D.	N.D.	N.D.
Dy	N.D.	N.D.	N.D.
Ho	<60	--	<500
Er	<50	N.D.	0
Tm	<50	<200	N.D.
Yb	<50	<50	<50
Lu	<10	N.D.	N.D.
La	<20	N.D.	N.D.
Sc	N.D.	N.D.	N.D.
Y	--	<300	<100

[a]Not detected.

necessary to reoxidize the sintered pellets back to the proper condition and to maintain that condition.

The reoxidation step was accomplished by placing the pellets in platinum dishes and heating to 1200°C in air for a period of 24 hours. While the entire pellet may not have been stoichiometric, a layer deep enough to accommodate the diffusion profiles was present as shown by the work of Berard et al. [57] on the reoxidation behavior of rare-earth oxides. It is interesting to note that the pellets used in this study were far more stoichiometric than those used in the earlier study.

As previously mentioned, good interfacial contact is required in order to obtain valid diffusion results. In this

study, it was reasoned that good contact could be obtained if both halves of the diffusion couple were polished optically flat before forming the couple. The procedure consisted of, first, the preparation of flat surfaces and, secondly a test to determine the degree of flatness.

The preparation step began with the mounting of the reoxidized pellets for polishing. The pellets were mounted in specially designed polishing cylinders (Figure 4) with type WI green rigidax wax (M. Arguesco & Company). To mount the specimen the specimen, mounting cylinder, small hexnut weight, and wax were heated on a hot plate to 100°C. Then, the pellet was placed on a glass microscope slide while the cylinder was elevated from the slide by spacers consisting of strips of glassine weighing paper. With the cylinder and specimen in this configuration the hexnut weight was placed on top of the pellet and melted wax was poured inside the cylinder.

Once the wax had set the polishing cylinder was removed from the glass slide and mounted in a Buehler polishing holder. The specimen was then polished on a Buehler vibramet polisher surfaced with Buehler uniwax using a 0.3μ alumina.

The purpose of the wax was to provide a napless polishing surface thus reducing the tendency for rounding.

Once the polishing was complete, the pellets were

Figure 4. Specimen waxed in mounting cylinder

Figure 5. Centorr furnace used for sintering and diffusion annealing

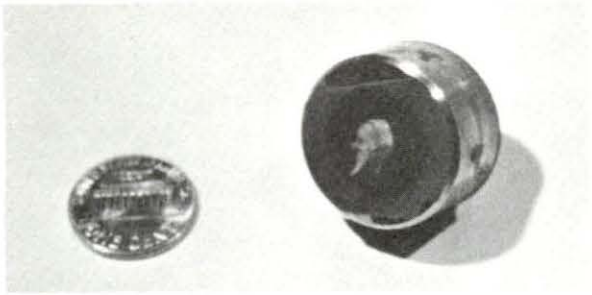

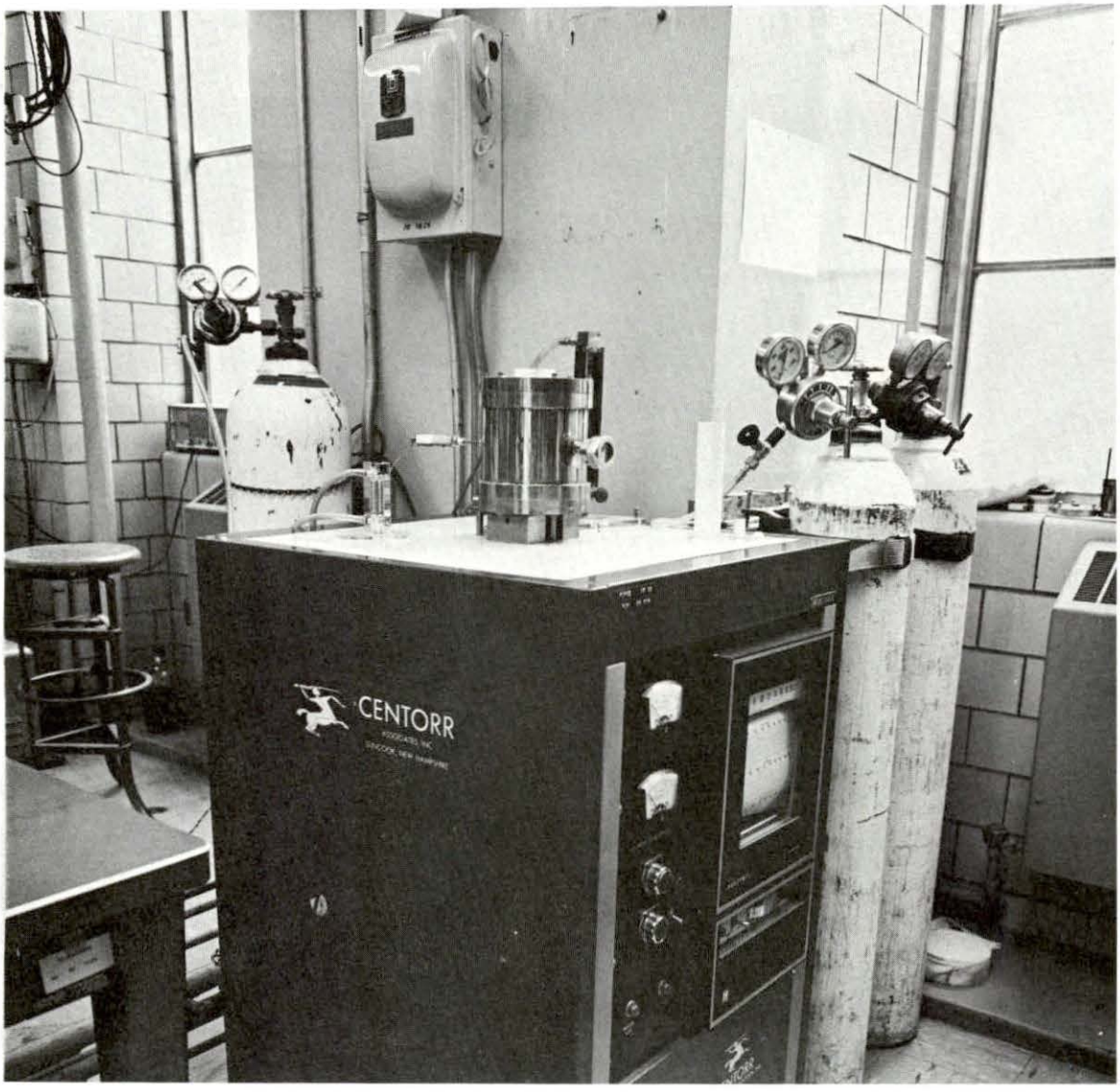
CENTORR

examined for flatness. Prior to this test the specimens were ultrasonically cleaned to remove loose alumina polish. The flatness of each pellet was then tested by means of an optical flat (obtained from Edmund Scientific Co. and flat to within 0.1 λ of the light used) and sodium light. With few exceptions, examination of the curvature and spacing of the resulting interference lines revealed that a single polishing gave the desired flatness.

With the individual pellets prepared and optically flat they were then ready for mating and diffusion annealing. In order to prevent loss of contact during insertion into the furnace, each couple was wrapped with a strand of Pt-Rh wire. The exception to this procedure was the anneal above the 1800°C vaporization temperature of Pt-Rh wire. At each temperature a total of six couples were annealed including three Y_2O_3-Er_2O_3 couples and three Ho_2O_3-Er_2O_3 couples. To prevent contamination, the couples were so placed that the Er_2O_3 sides rested on an Er_2O_3 crucible.

For the diffusion anneals two separate furnaces were used. The low temperature (1380°C) run was made in an alumina tubed glow bar furnace. Control of this furnace was by means of a thermocouple but the specimen temperature was measured by means of a Pt vs Pt 10% Rh thermocouple. The higher temperature diffusion anneals were conducted in the Centorr furnace (Figure 5). In order to operate in an oxidizing environment,

the furnace was set up with an impervious zirconia muffle tube. Control of the Centorr was by means of a thermocouple (W 5%Re vs W 26%Re) however the specimen temperature was measured by means of an optical pyrometer. Argon flowed around the outside of the muffle while oxygen was trickled through the muffle to maintain stoichiometry of the specimens throughout the anneal.

Once the diffusion anneal was complete the specimens were mounted in Acrylic and polished parallel to the diffusion direction with 600 grit silicon carbide, 1μ diamond and 0.3μ Al_2O_3. The polished couples were then ultrasonically cleaned to remove the polishing grit and coated by vapor deposition with a thin layer of carbon. The coated specimens were submitted to an electron microprobe analysis on a Hitachi Perkin Elmer XMA-5 Electron Probe microanalyzer. The analysis consisted of scanning for 20 sec along an 80 micron line maintained perpendicular to the diffusion direction. The intensity of $L\alpha$ lines from the elements of interest were used to provide the concentration information. Distances were chosen so as to avoid any pores present. The resulting data were in the form of counts per 20 seconds interval for the interdiffusing elements as a function of distance. These data were then converted to atomic percent using MAGIC a computer program for quantitative electron microprobe analysis (written by J. W. Colby of Bell Telephone Laboratories, Inc., Allentown, Pennsyl-

vania). Resulting from this conversion was a profile (atomic percent Er vs distance in microns) which was analyzed by the Matano method using a fitting technique described by Doyle [70]. The penetration plot was divided into three sections for fitting purposes. Each section was fitted separately using any needed polynomial up to degree five. Upper and lower sections were then integrated to yield upper and lower areas. Upper and lower areas were then coupled with the center section polynomial to determine a Matano interface. Finally a diffusion time was introduced and diffusion coefficients were calculated at specified concentrations. As noted before, justification for the use of the Matano analysis is based on the small variation in molar volume with composition in both the Er_2O_3-Y_2O_3 and Er_2O_3-Ho_2O_3 systems.

Additional Investigations Relating to Specimen Preparation

The specimen preparation developed in this study has resulted largely due to occurrence and investigation of certain interrelated phenomena. While some of these effects are not peculiar to the rare-earth oxides, it is nevertheless helpful to discuss their significance in developing the preparation methods used.

Initially the pellets were machined from large cylinders of hot pressed material. Hot pressing seemed attractive because of its capability of producing high density material. Indeed hot pressing at 1600°C and 4000 psi gave densities

well above 99% of the theoretical values. However when diffusion couples, prepared from this material, were heated to temperatures above 1600°C such undesirable effects as warpage and intergranular cracking were observed. As a result of the warpage, interfacial contact was broken preventing the use of the diffusion couples for generation of data. Even the use of data taken in the neighborhood of points found in contact at the end of the diffusion anneal was not considered advisable since there was no assurance that even in this region contact had been maintained throughout the run. The problem of warpage represented no new and startling problem in ceramics so it appeared that a simple solution could be obtained. Giving careful consideration to all the possible solutions to the warpage problem the following three options were found consistent with the goals of this study.

1. Hot pressing at higher temperatures.
2. Annealing hot pressed material (1600°C) at a higher temperature, then polishing to flatness.
3. Cold pressing, isostatically pressing and sintering at a higher temperature.

The higher temperature mentioned above refers to a temperature higher than the hottest diffusion anneal.

A second problem observed in the hot pressed material diffusion annealed above 1600°C was that of intergranular cracking. Material examined before the anneal and found to

be highly dense was full of intergranular cracking after the anneal. It is conceivable that during hot pressing strains were introduced which were relieved upon heating above the hot pressing temperature. This relief of strains then could have manifested itself as a kind of pulling apart of the grains. At any rate this second problem further demonstrated that material hot pressed at 1600°C was not satisfactory for this study.

On the basis of the unsatisfactory results from the 1600°C hot pressed materials, attempts were made at higher hot pressing temperatures. As the temperature went up, so did the reaction rate with the graphite die. At 1850°C, reaction with the graphite die was complete resulting in the total loss of the starting material. The generally unsatisfactory results of these attempts to hot press above 1600°C, led to the abandonment of this method of specimen preparation.

The second alternative, that of annealing above the hot press temperature and afterwards polishing to flatness, was tried and another undesirable phenomena, bloating, was observed. This macroscopically observable bloating, observed at temperatures above 1800°C, manifested itself in the form of what appeared to be surface bubbles and internal caverns.

It was reasoned that the bloating behavior could be due to the evolution of an internally trapped impurity. The impurity could have originated in either the "as received"

material or have been pressed in during the hot pressing step. The fact that bloating also occurs in cold pressed and slip cast material as well, tended to support the impure-starting-material premise. For this reason the reprecipitation step was undertaken. When reprecipitated and calcined material was stored too long (under ascarite and anhydrone) before sintering and annealing, it too bloated. These observations, directed attention towards the heating cycle during sintering. The reasoning was that, if too rapid a heating rate was used, a surface "skin" could form preventing outgassing of the impurities. By heating to 1400°C and holding to allow for outgassing, bloating was eliminated.

In order to gain a greater understanding of bloating effects, bloated specimens were subjected to a S.E.M. (scanning electron microscope) examination. Figures 6, 7, 8, 9 and 10 are S.E.M. photographs taken of bloated specimens using the JSM-U3 instrument. Examination of these photos reveals much interesting information.

All specimens in Figures 6 through 10 were fabricated by hot-pressing (1600°C and 4000 psi) and annealed at 1900°C for 5 hours. In preparation for the S.E.M. analysis each specimen was polished with 0.3μ Al_2O_3 and then ultrasonically cleaned. Coating used involved first a carbon coat then a 40% Au-60%Pd layer.

Figure 6 is a view within "a bloat" in Ho_2O_3. Rather

Figure 6. (top left) Bloated Ho_2O_3 magnification; 1000X

Figure 7. (top right) One end of lower left rod in Figure 6; magnification 3000X

Figure 8. (center left) End-on view of lower left rod in Figure 6; magnification 3000X

Figure 9. (center right) Bloated Y_2O_3; magnification 1000X

Figure 10. (bottom) Er_2O_3 specimen; magnification 1000X

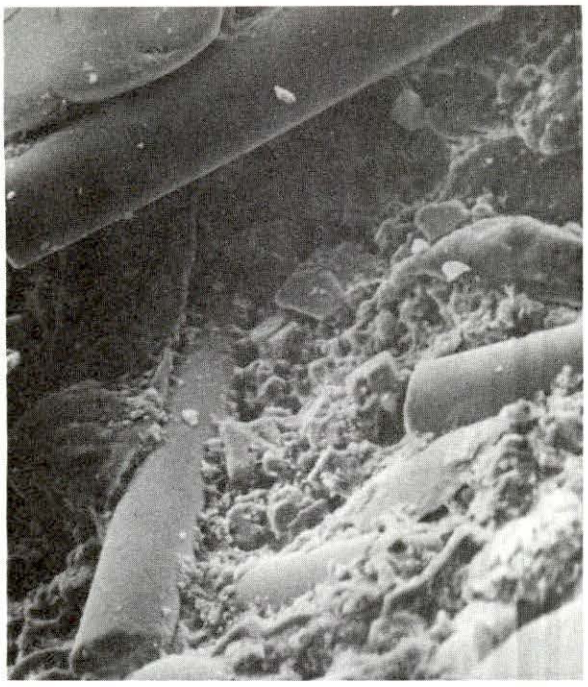

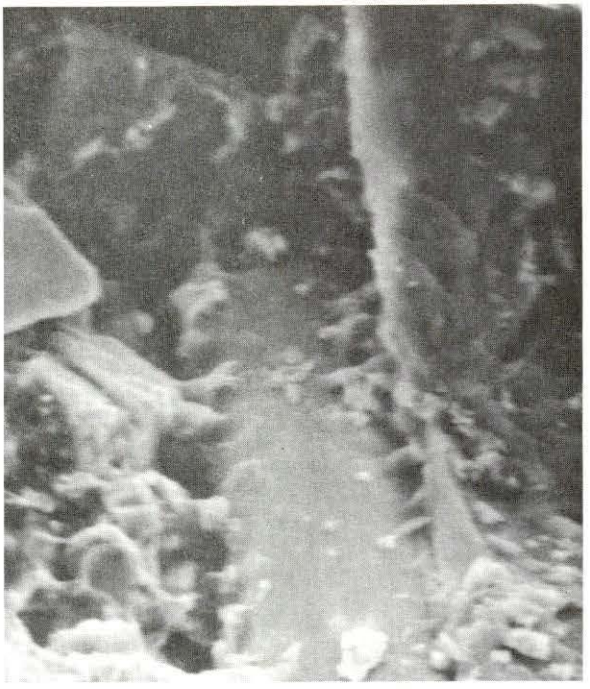

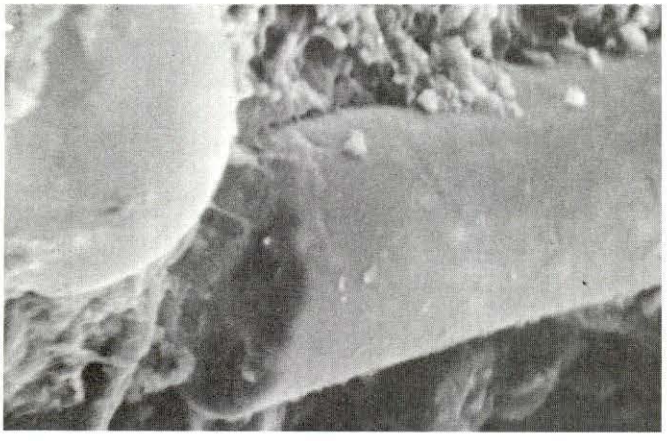

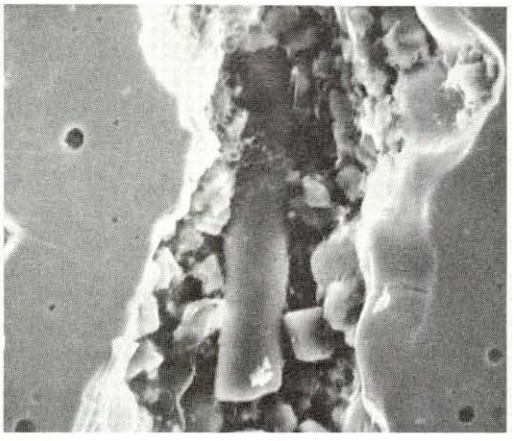

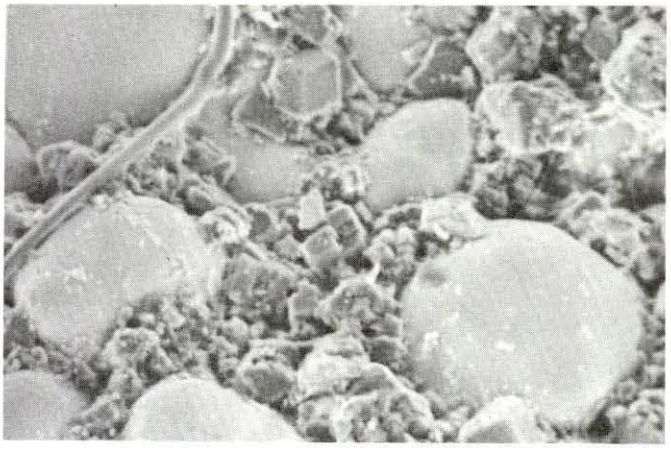

massive rod-like structures seem to be well imbedded in the matrix. Likewise the general structure within the void appears very different from what would be expected from a polished polycrystalline specimen. Figure 7 shows a magnified view of one end of the rod seen in Figure 6 and shows that the rods are definitely incorporated within the matrix material rather than lying on the surface. Figure 8 shows a magnified view of the other end of the same rod.

The apparent difference in structure of the rods leads one to consider the possibility of a difference in composition. With this idea in mind the rod shown in Figure 9 was subjected to an electron probe analysis using the S.E.M. which revealed no significant compositional difference between rod and matrix material. For example the rod in Figure 9 was found to contain Mn, Ge, P, Ar, Cu, Zn, Y, and Sr while the matrix consisted of Mn, Ge, P, Ar, Cu, Ni, Fe, Zn, Ta, Tl, and Y. In viewing Figure 9 two other observations can be made. First, if gas evolution was the cause of bloating, spherical voids (low free energy configuration) would be expected. However the voids are far from spherical and, in fact, seem more like cracks. The second observation is that a cubic structure is clearly indicated within the void.

Figure 10 shows a view of another location in an Er_2O_3 specimen. Again, a cubic structure is indicated with rounded structures also present. Possibly the phenomenon here is one

of cracking followed by preferential coalescence (represented by spherical structures).

The investigation of bloating resulted in the successful elimination of the problem as it affected this study but it is clear that a detailed understanding of the bloating phenomenon requires further work. One could postulate that the formation of the rods and spheres is a consequence of a preferred growth direction. However the connection between rods, spheres and bloating does not seem clear at this time.

One additional comment should be made with regard to the X-ray analysis of the bloated material. The presence of Ar is an interesting observation. These data indicate that the C-fluorite rare-earth structure is capable of deforming so as to accommodate the Ar atom. Generally Ar solution in materials is not expected due to its size, however evidently the defective anion rare-earth structure is capable of dissolving Ar. The Ar dissolution may be significant to "bloating" since bloating has only been observed in specimens fired in argon.

RESULTS AND DISCUSSION

Profiles resulting from the diffusion anneals appear in Figures 11 through 27. Each profile displays the expected "S" curve shape. Both the experimental points and the least squares fitted curves are shown. In all cases but one, the fit appears quite good. A typical root mean square error calculation yields numbers from 1.2 atomic % units for concentrations above 10 atomic %, to 0.2 atomic % units for values below 10 atomic %. The exception if Figure 14 where a point at 225 microns falls far below the curve defined by the other points. The point in question was not used in the fitting procedure because of its effect on the shape of the profile. Use of the point would result in a dip which would adversely affect the Matano interface determination. No explanation for this point is offered other than a possible electron beam current fluctuation.

Figures 28 through 35 present the concentration dependence of D. A consistent trend is observed with D monatonically decreasing as pure Ho_2O_3 and pure Y_2O_3 conditions are approached in the systems Er_2O_3-Ho_2O_3 and Er_2O_3-Y_2O_3 respectively. At each temperature a straight line was fitted to the D vs concentration data using the method of linear least squares. Assuming that $D = mc + b$ applies, constants for the equations of these fitted lines are given in Table 2. The equations yield results good to no more than 3 significant figures.

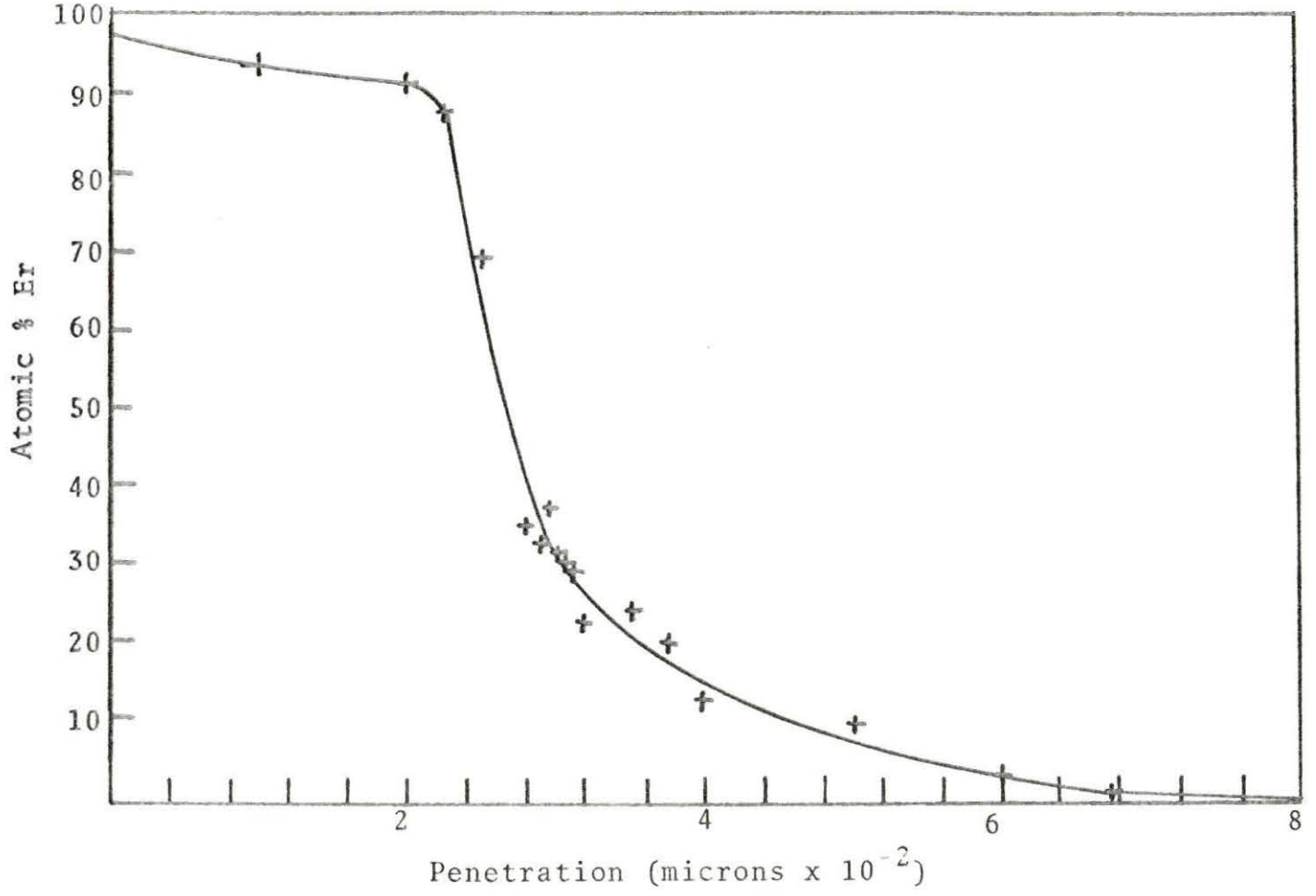

Figure 11. Er_2O_3-Ho_2O_3, 1890°C, 2 hr 15 min

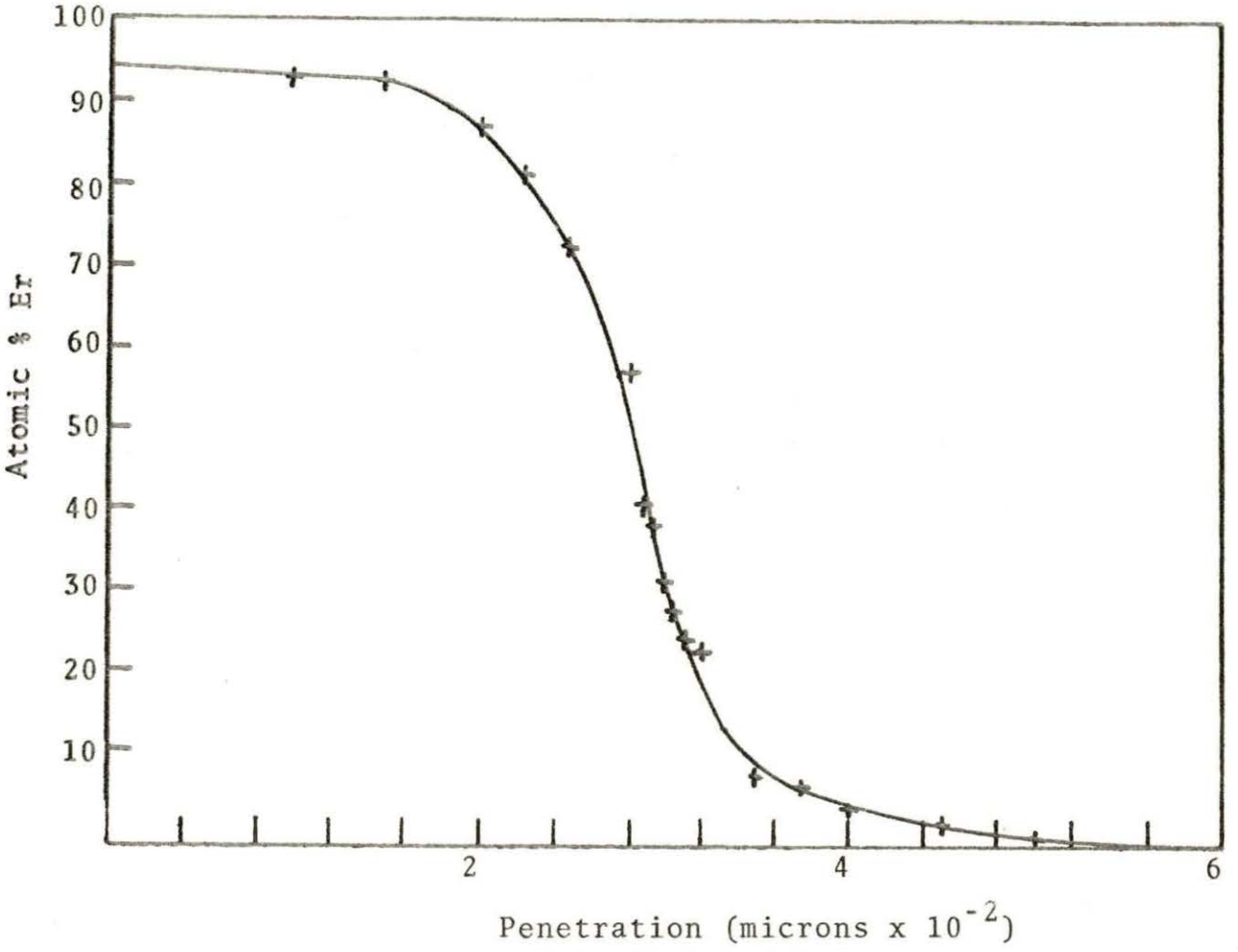

Figure 12. Er_2O_3-Ho_2O_3, 1890°C, 2 hr 15 min

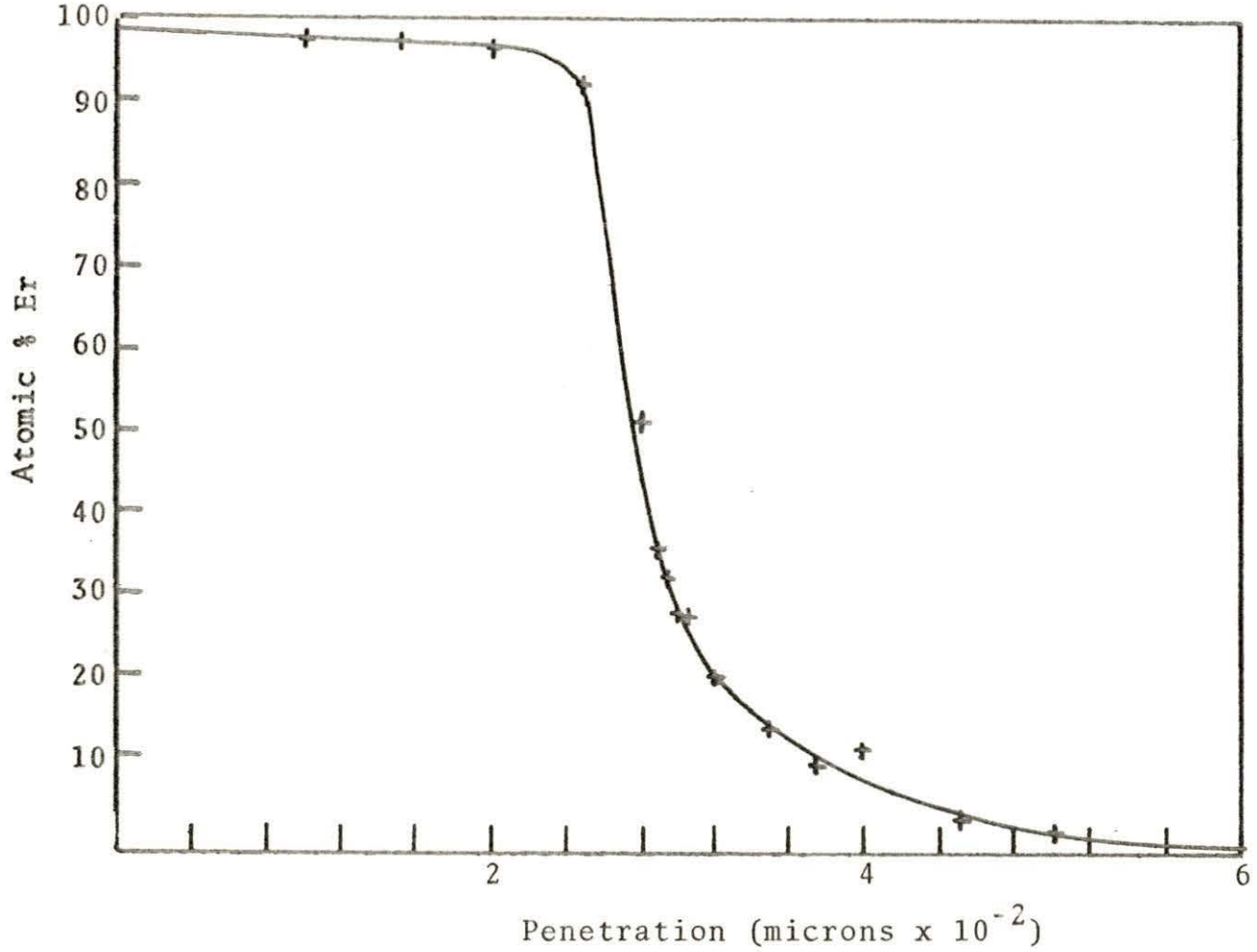

Figure 13. Er_2O_3-Ho_2O_3, 1890°C, 2 hr 15 min

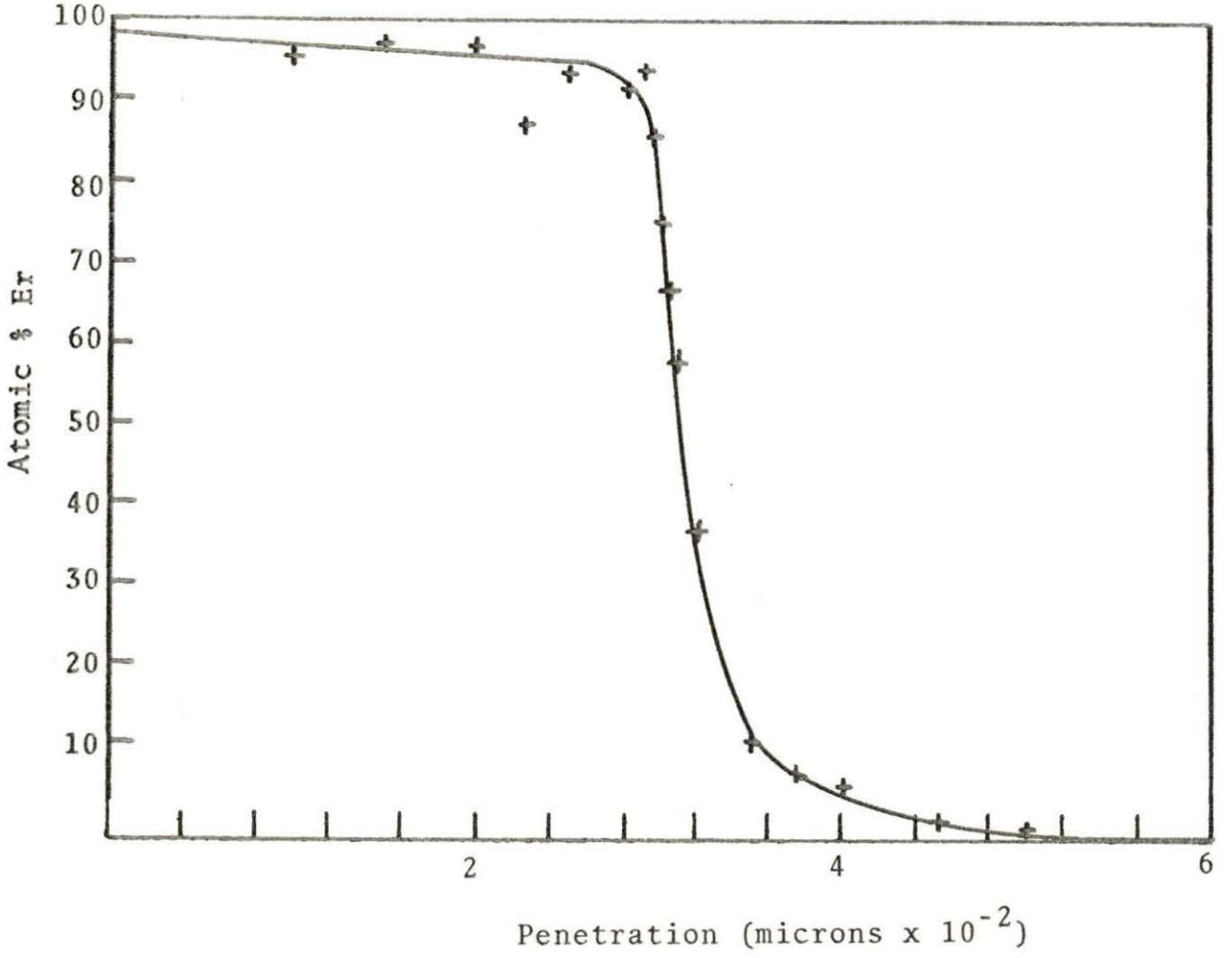

Figure 14. Er_2O_3-Y_2O_3, 1890°C, 2 hr 15 min

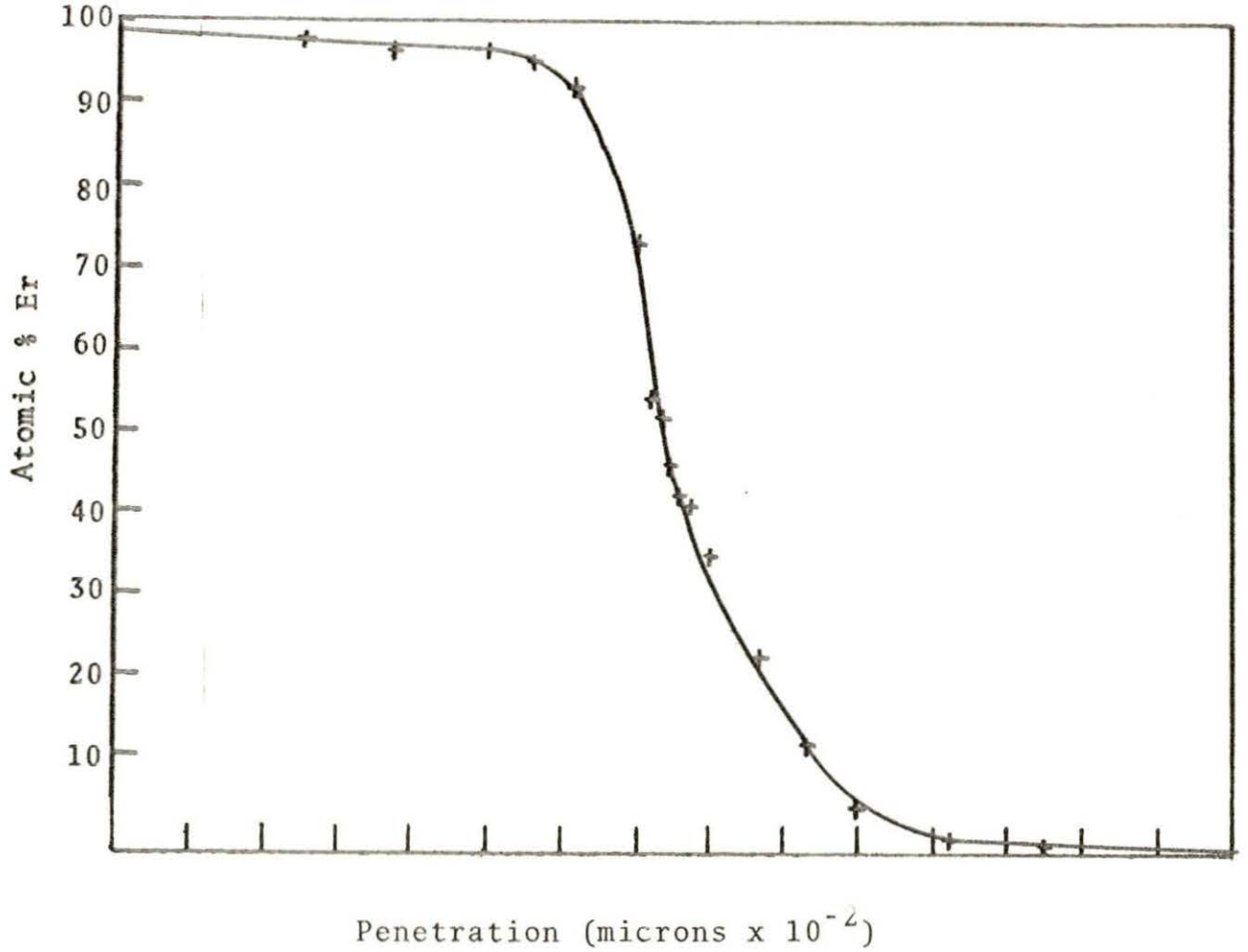

Figure 15. Er_2O_3-Y_2O_3, 1890°C, 2 hr 15 min

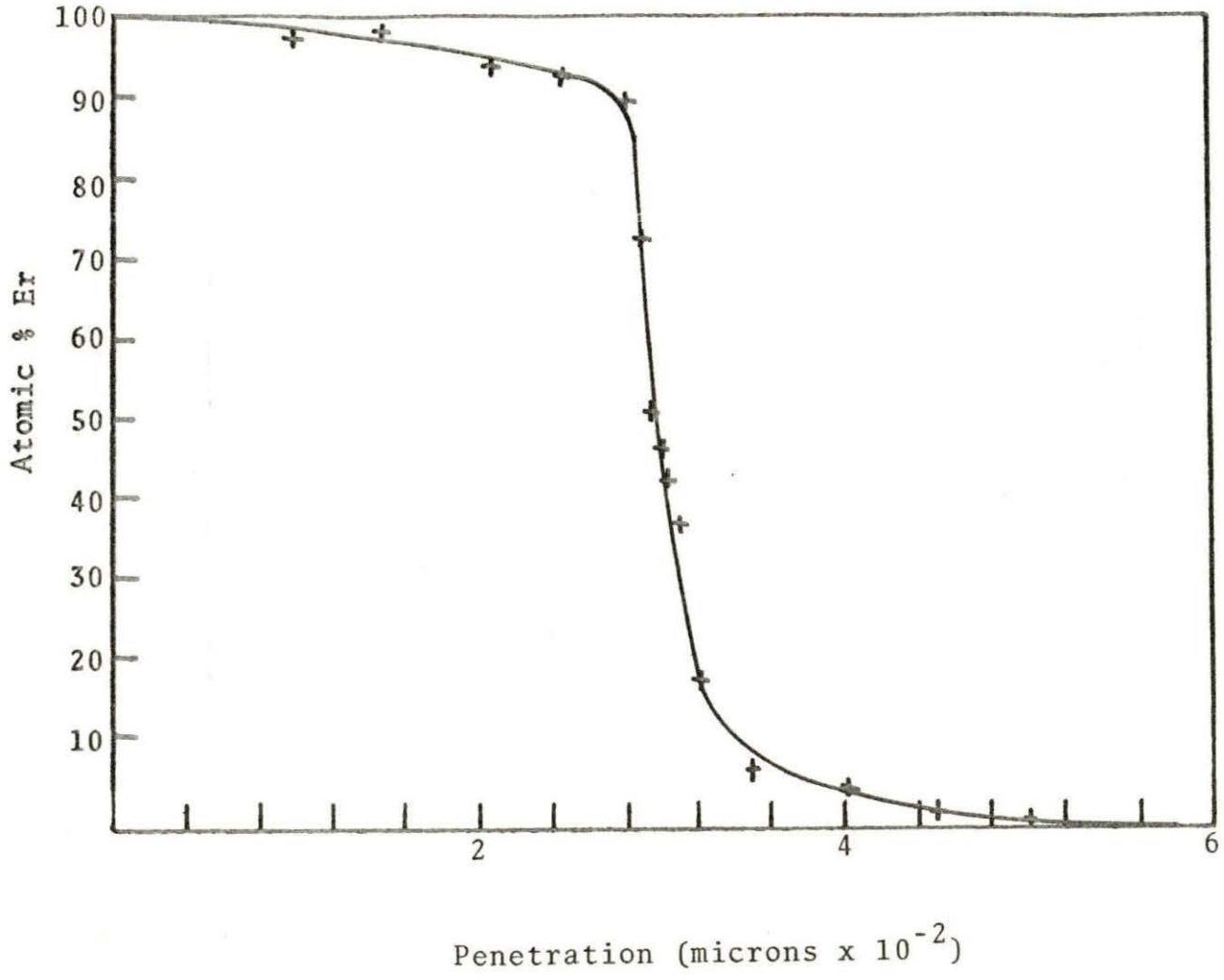

Figure 16. Er_2O_3-Y_2O_3, 1890°C, 2 hr 15 min

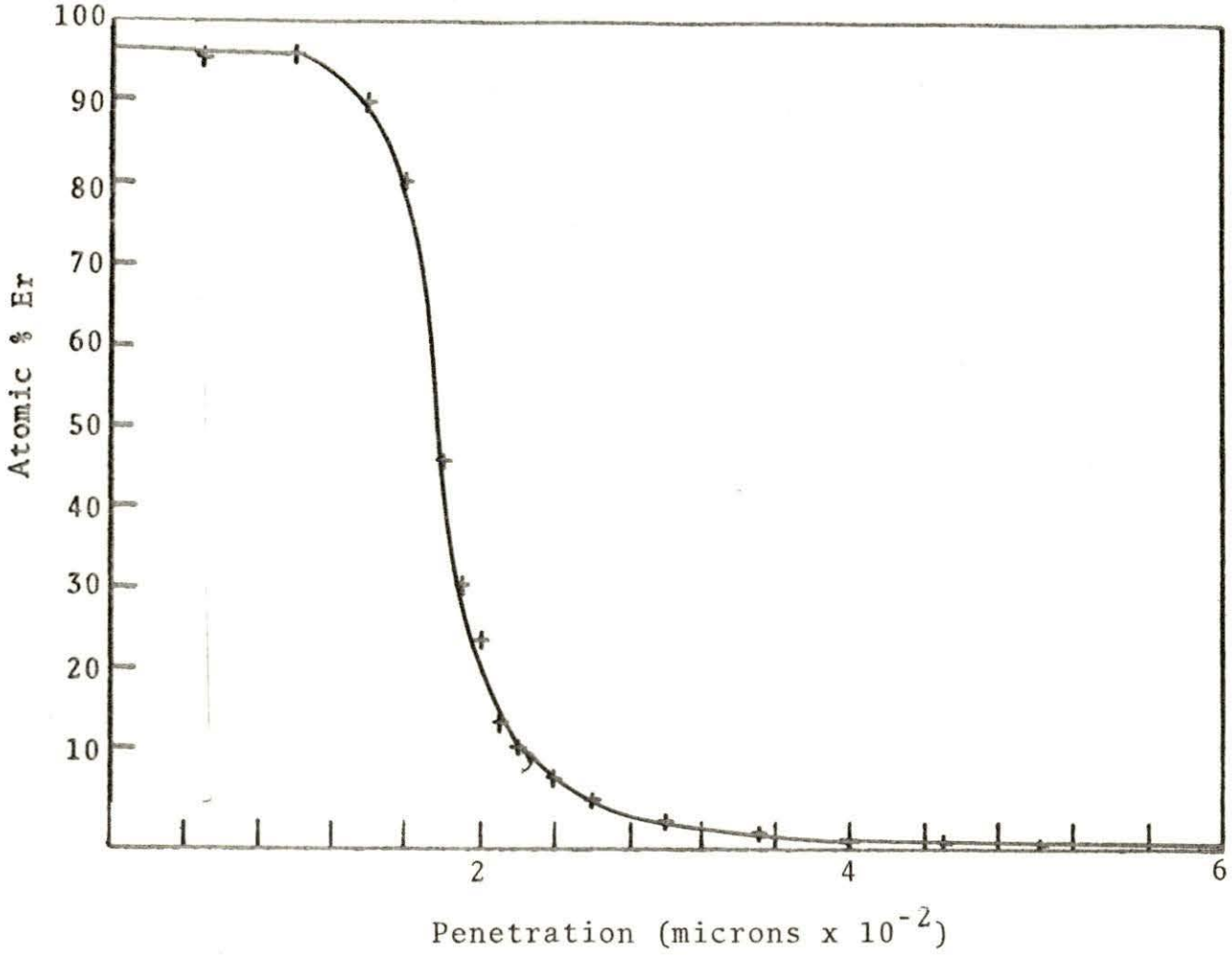

Figure 17. Er_2O_3-Ho_2O_3, 1780°C, 10 hr

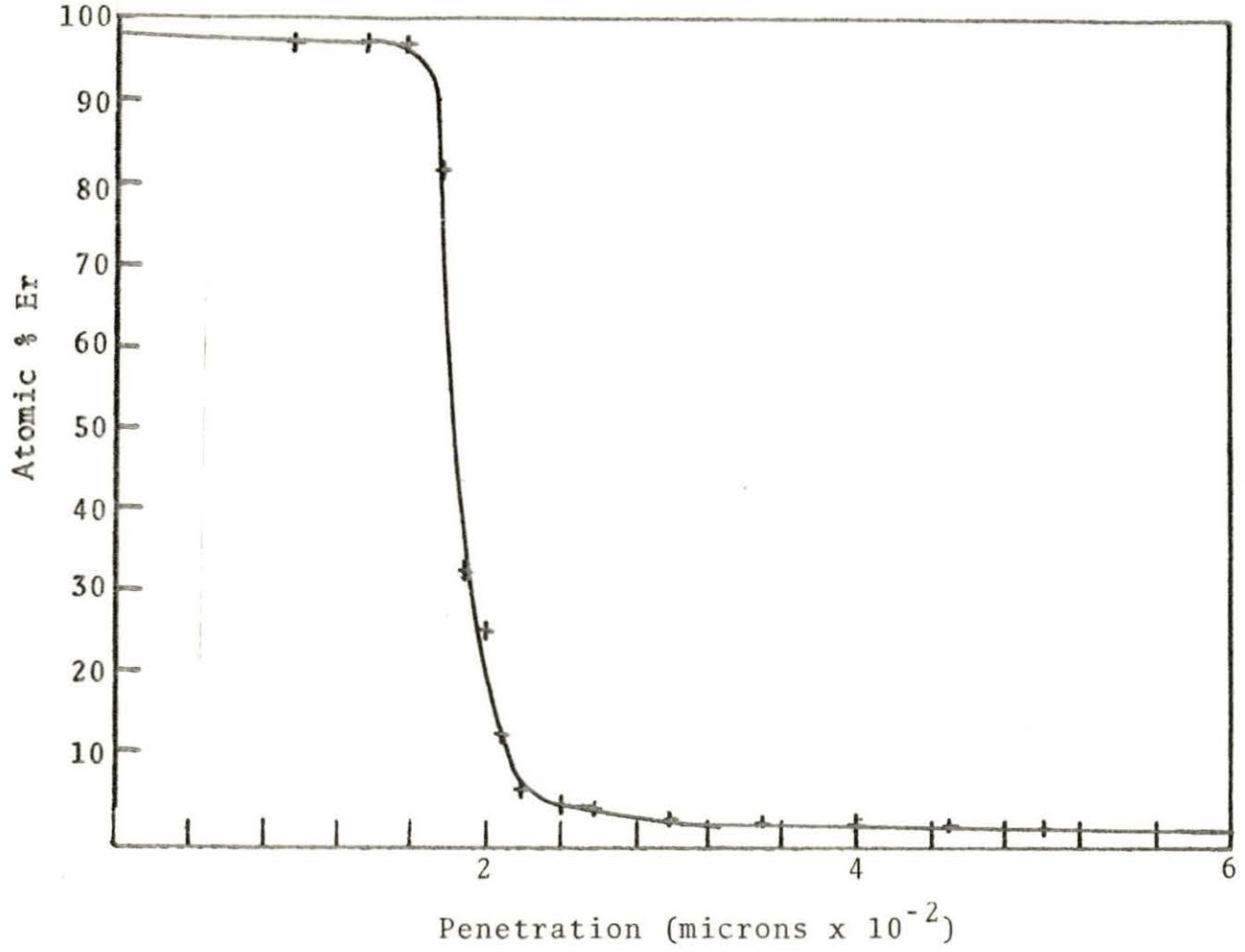

Figure 18. Er_2O_3-Ho_2O_3, 1780°C, 10 hr

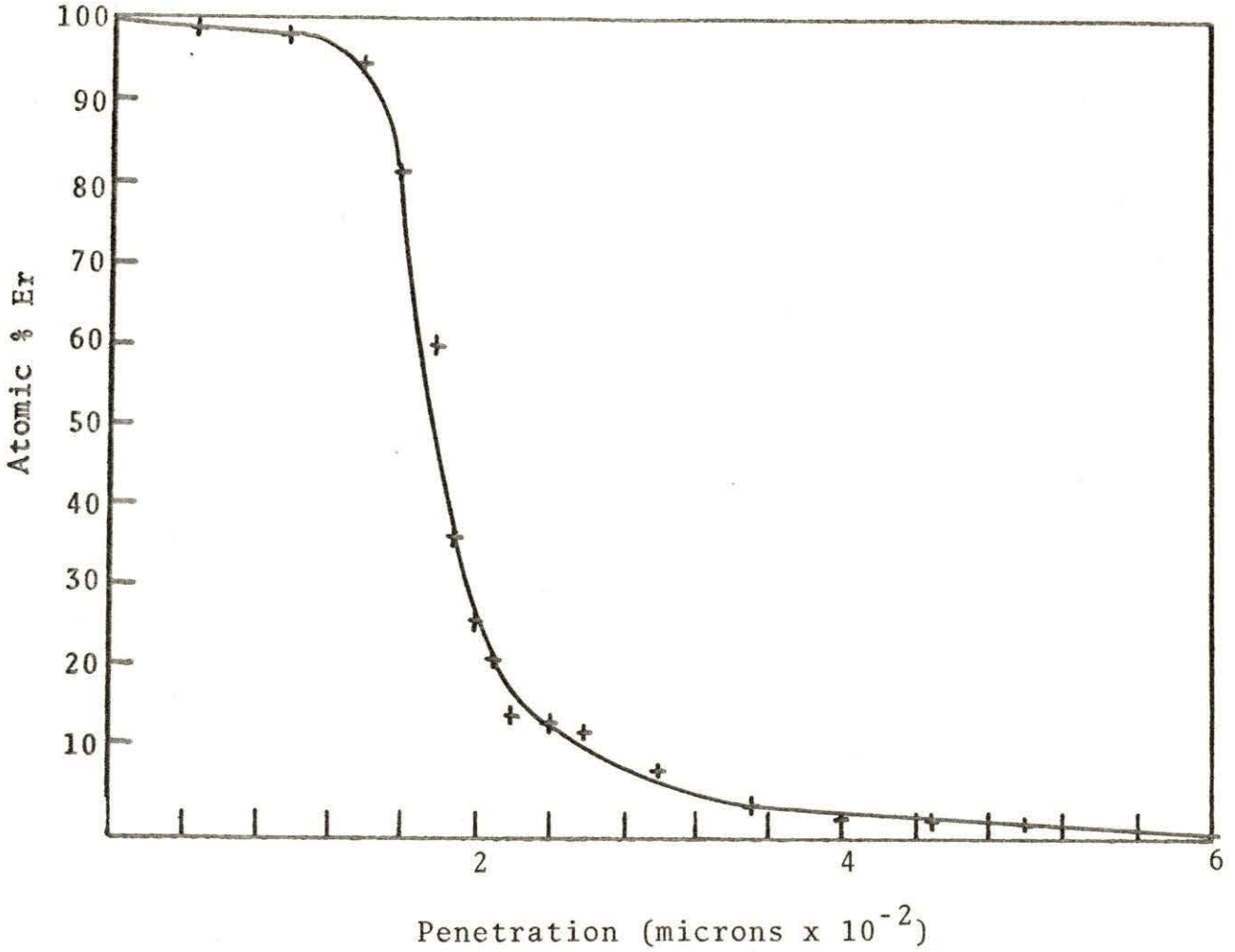

Figure 19. Er_2O_3-Ho_2O_3, 1780°C, 10 hr

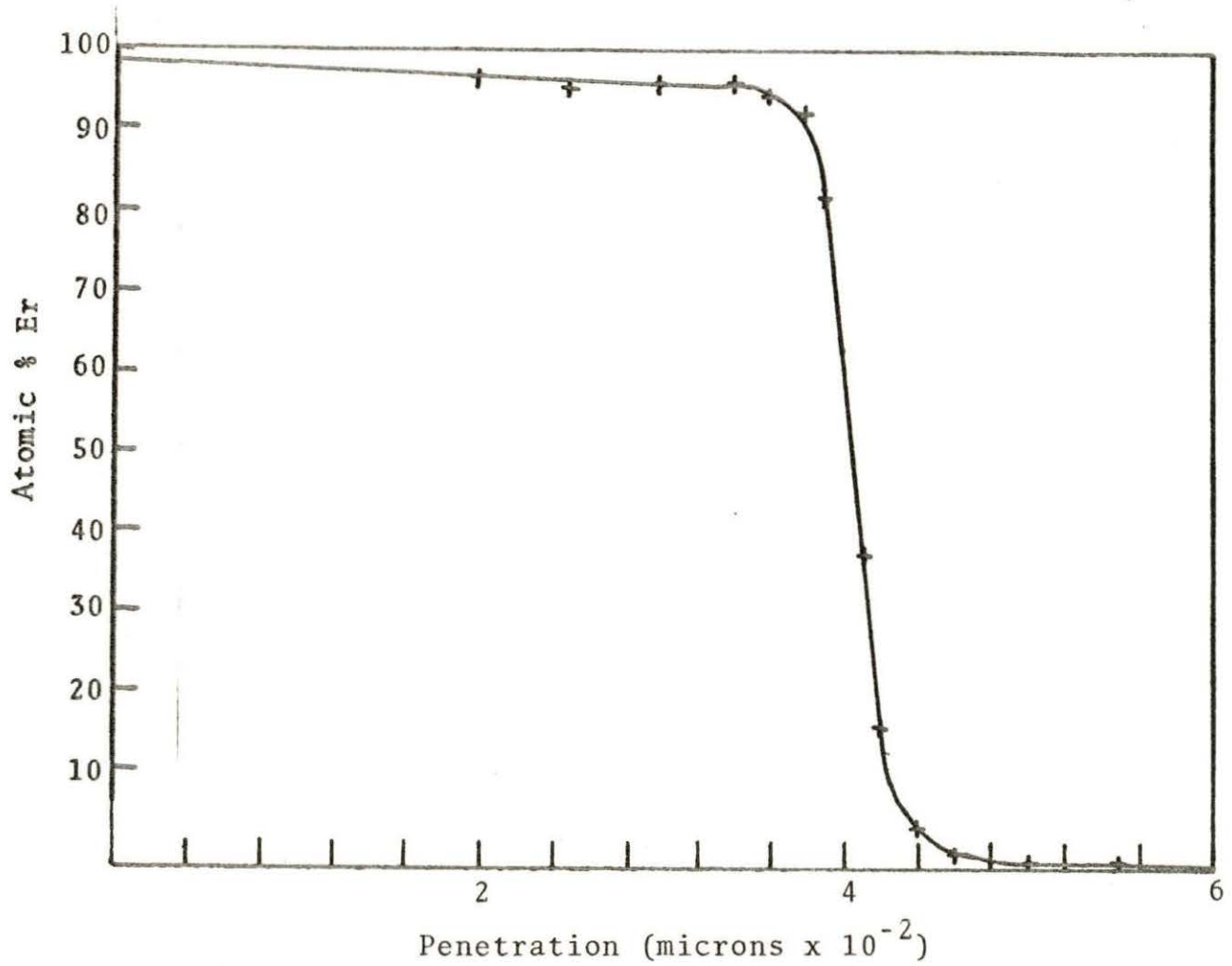

Figure 20. Er_2O_3-Y_2O_3, 1780°C, 10 hr

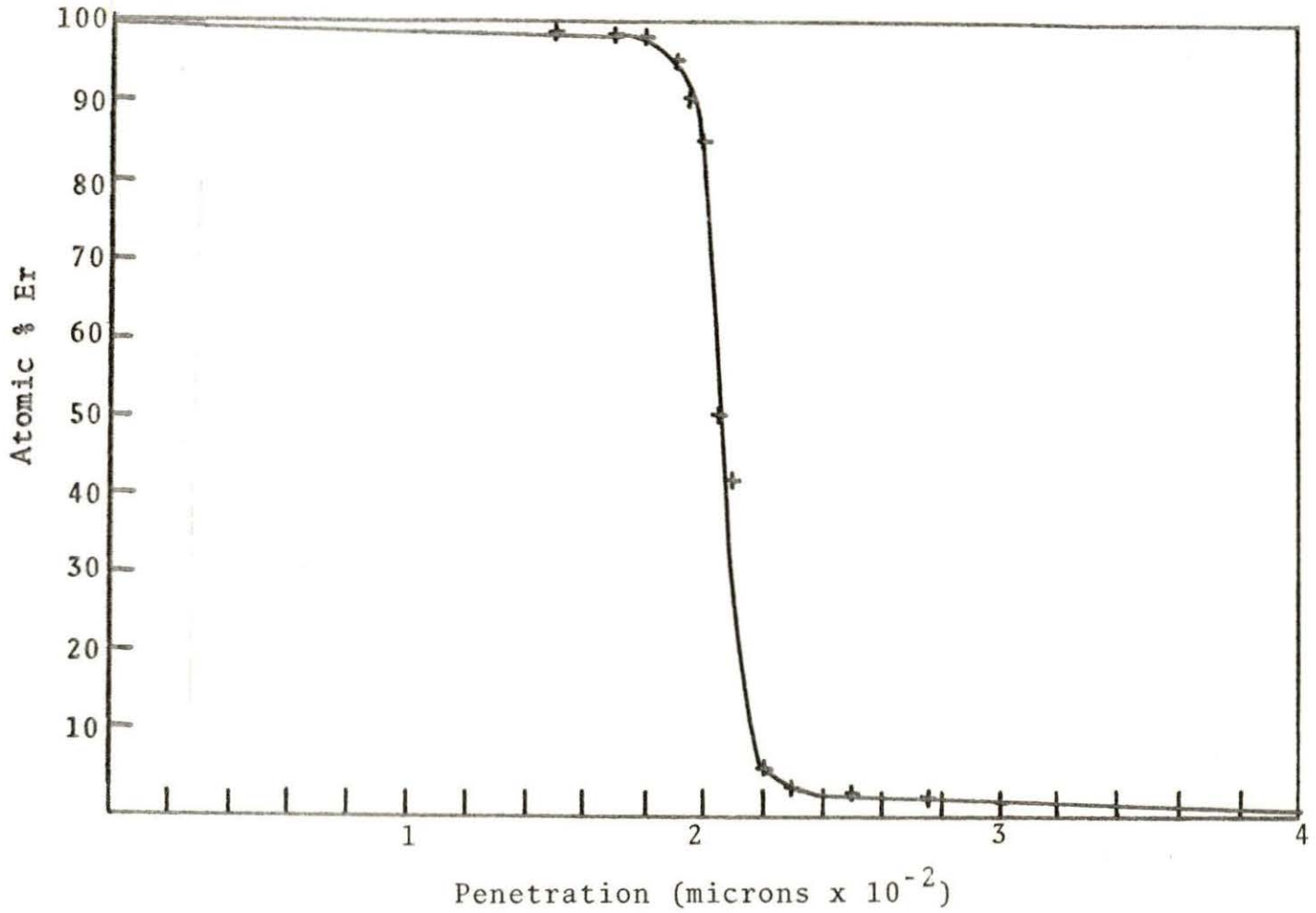

Figure 21. Er_2O_3-Y_2O_3, 1780°C, 10 hr

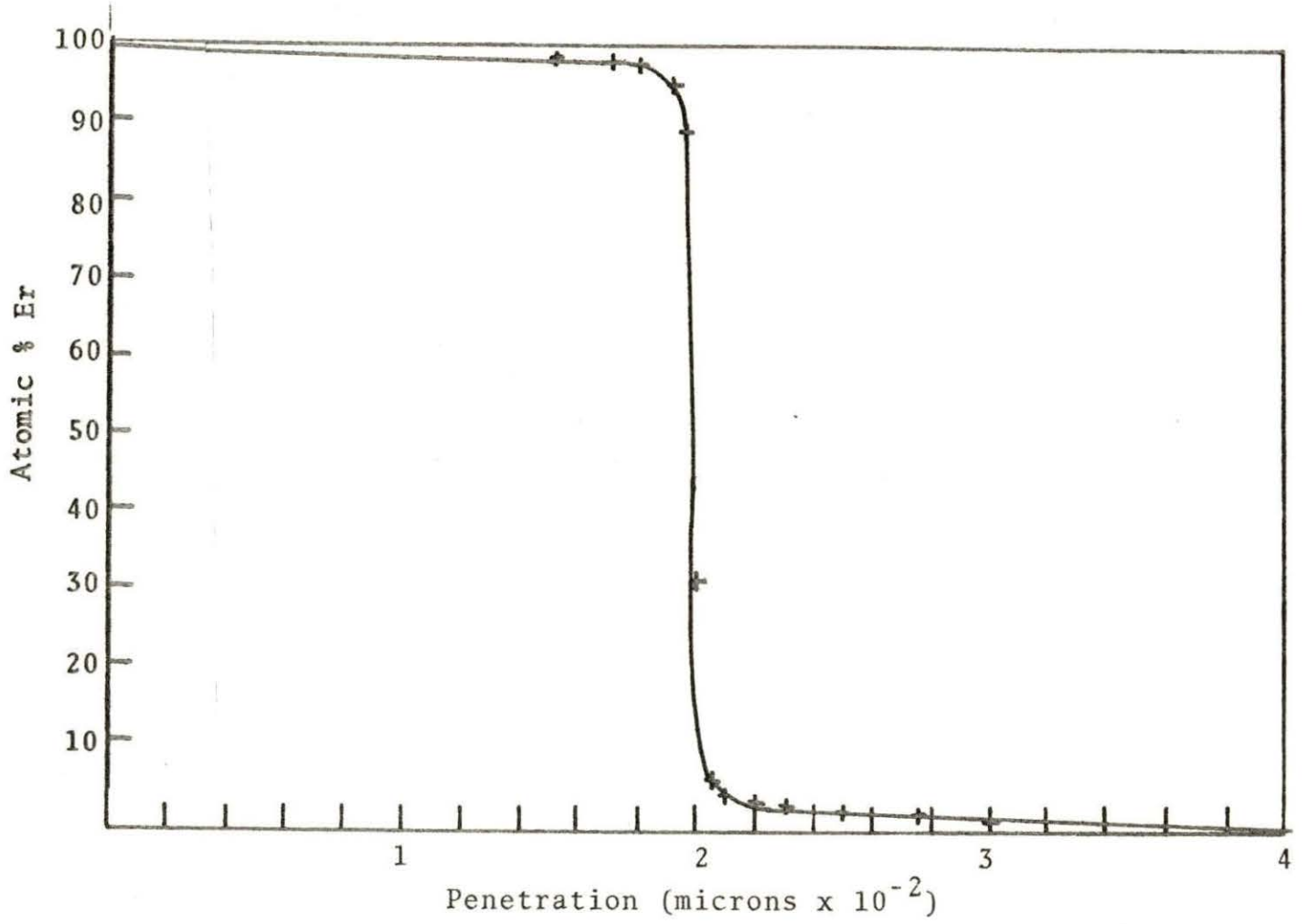

Figure 22. Er_2O_3-Y_2O_3, 1780°C, 10 hr

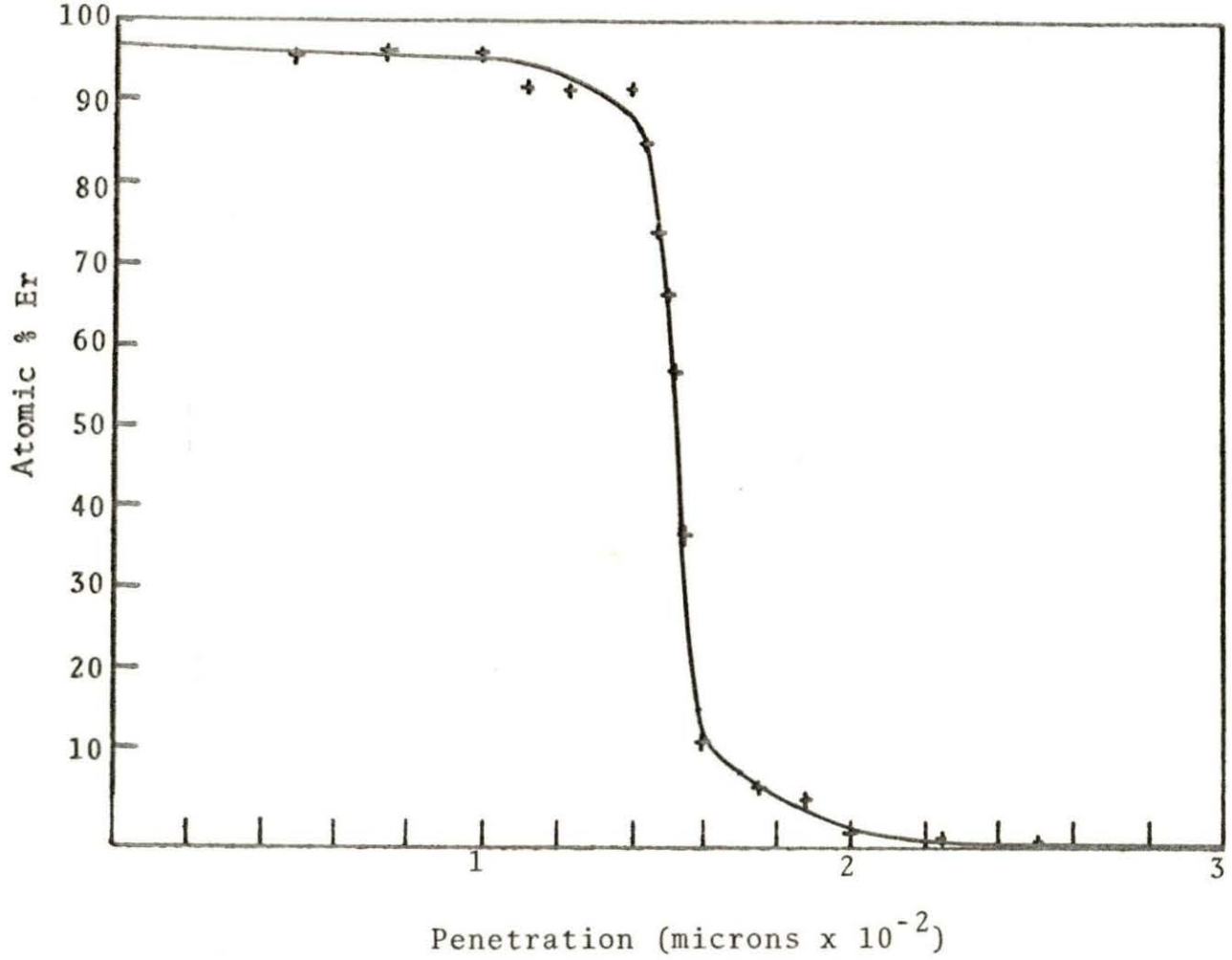

Figure 23. Er_2O_3-Ho_2O_3, 1700°C, 16 hr

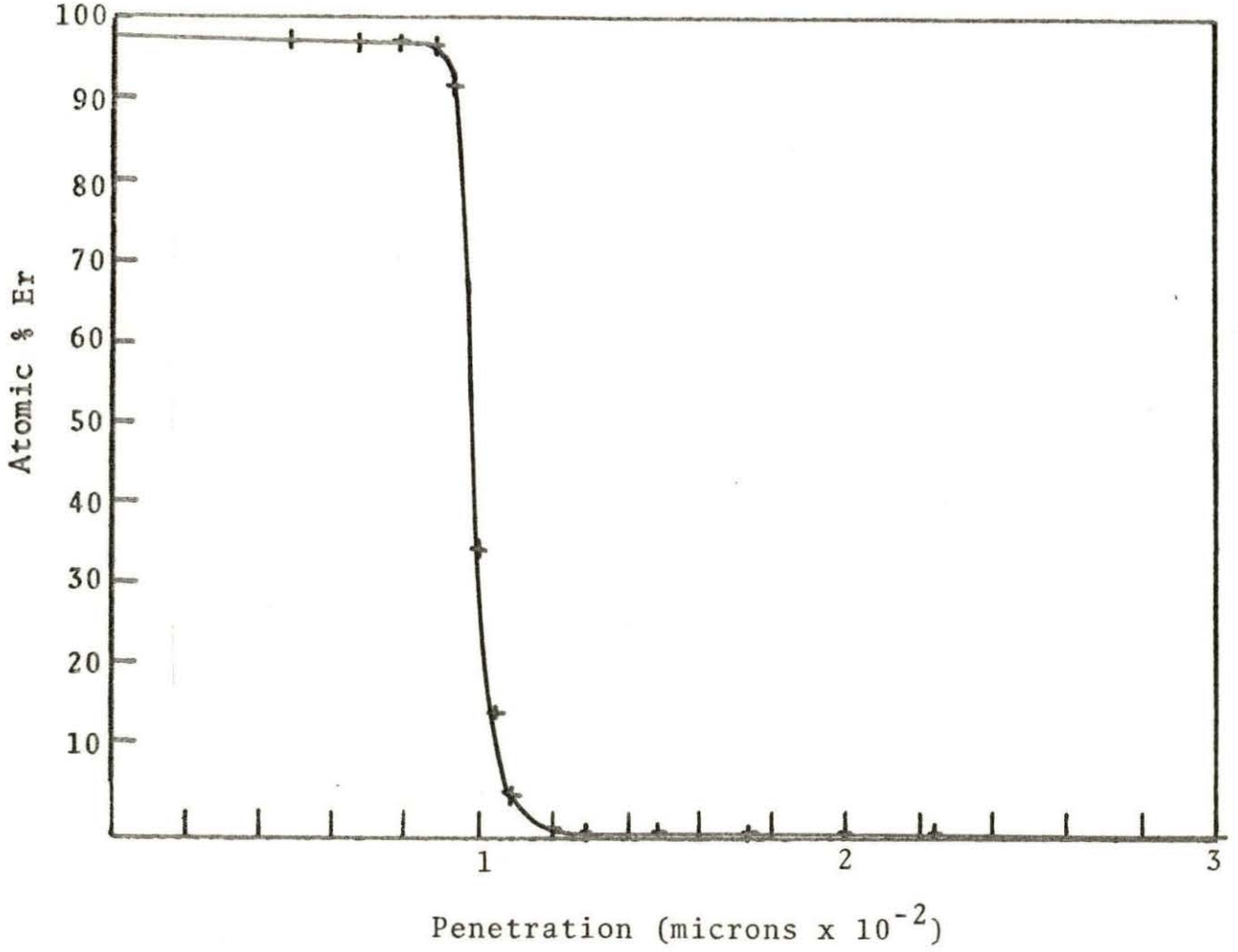

Figure 24. Er_2O_3-Y_2O_3, 1700°C, 16 hr

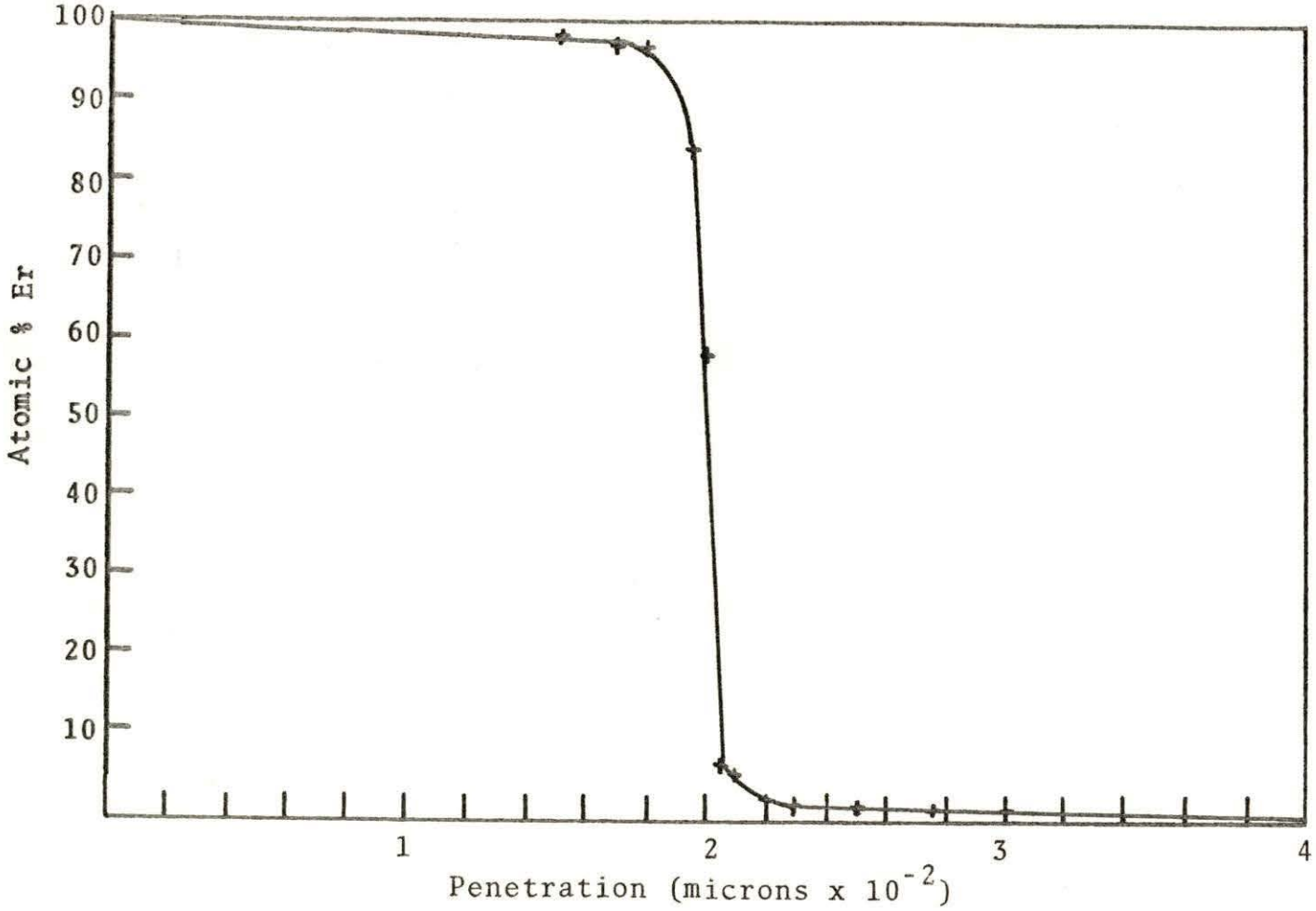

Figure 25. Er_2O_3-Y_2O_3, 1700°C, 16 hr

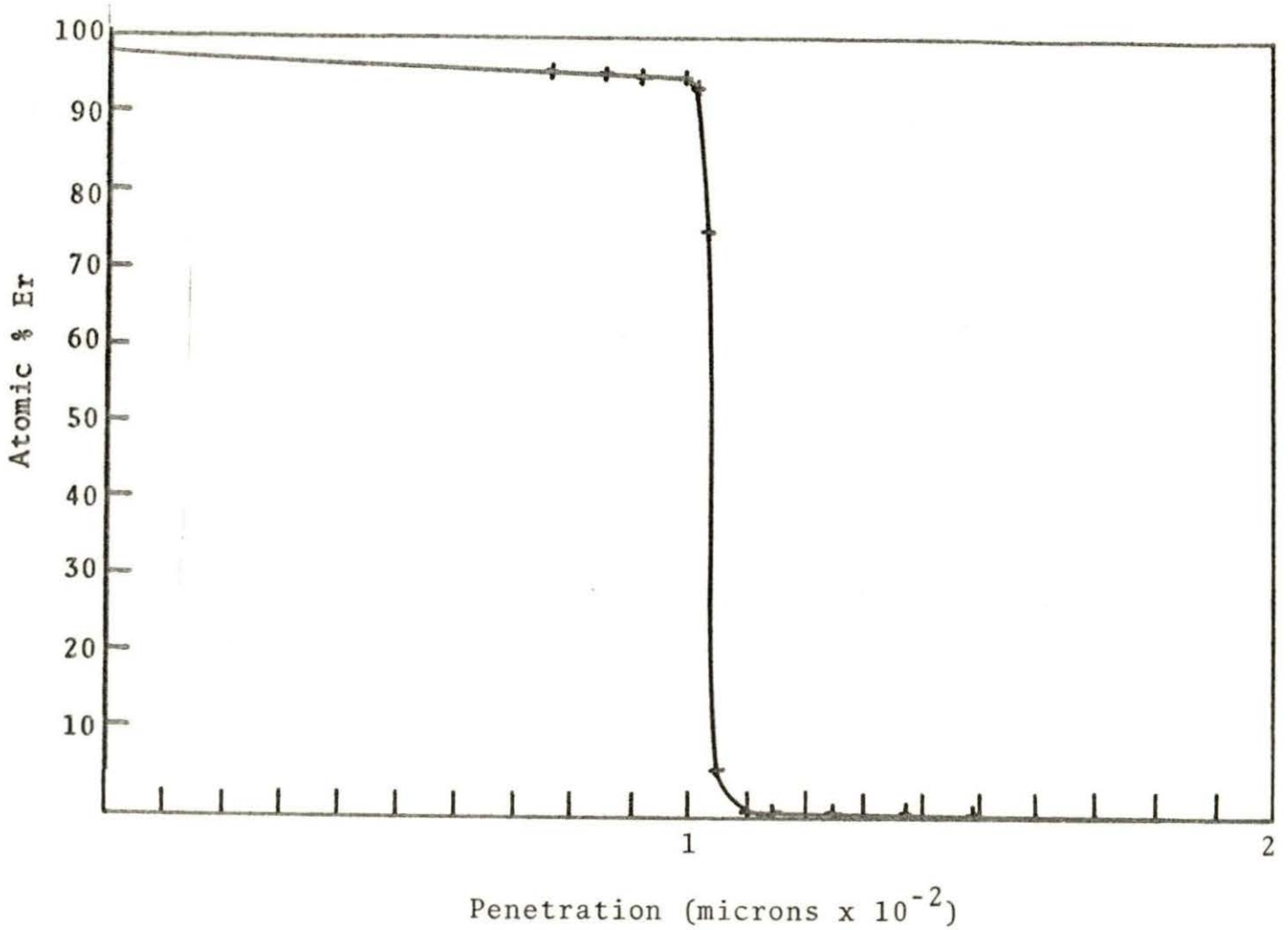

Figure 26. Er_2O_3-Y_2O_3, 1400°C, 23 day 14 hr 40 min

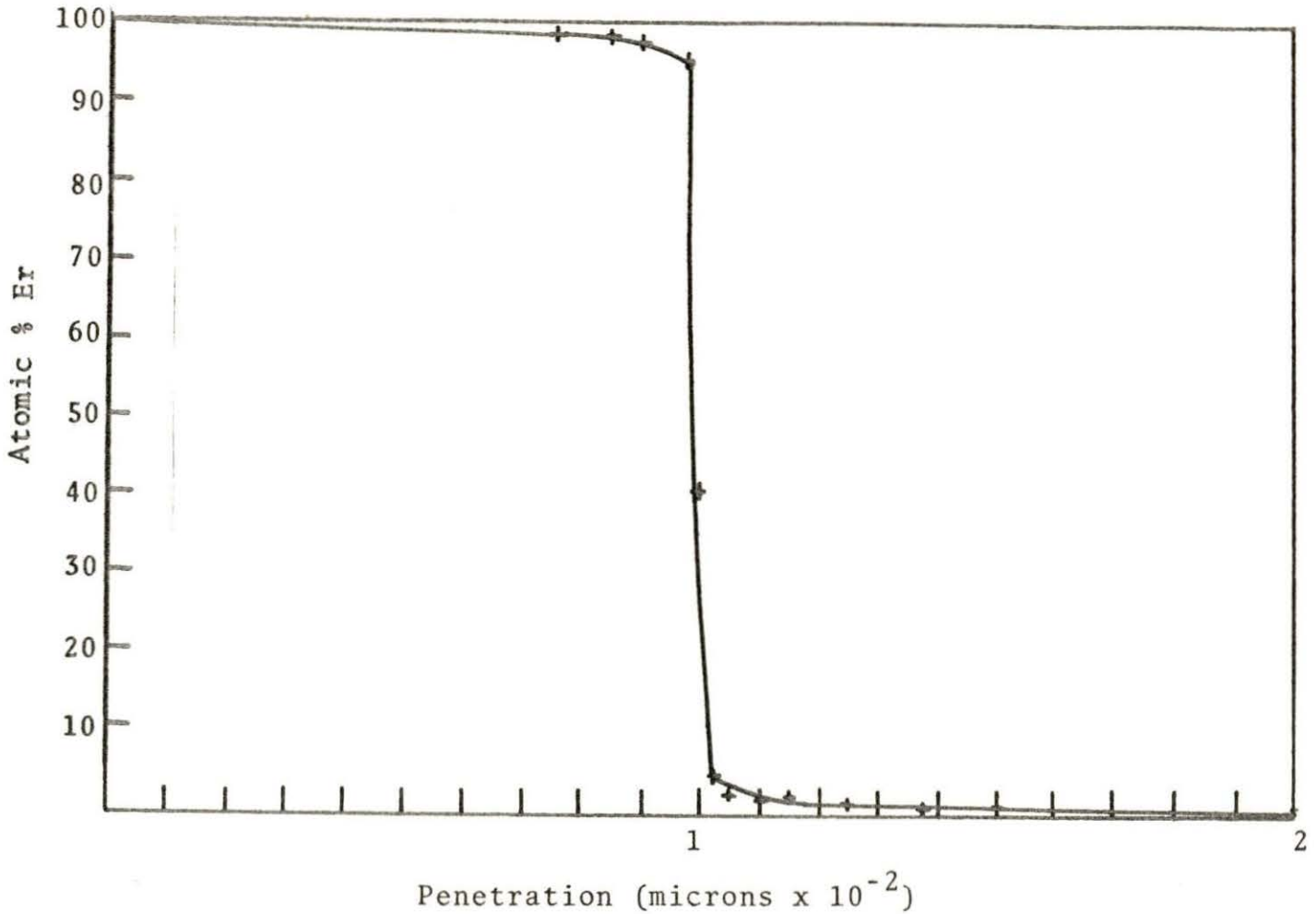

Figure 27. Er_2O_3-Ho_2O_3, 1400°C, 23 day 14 hr 40 min

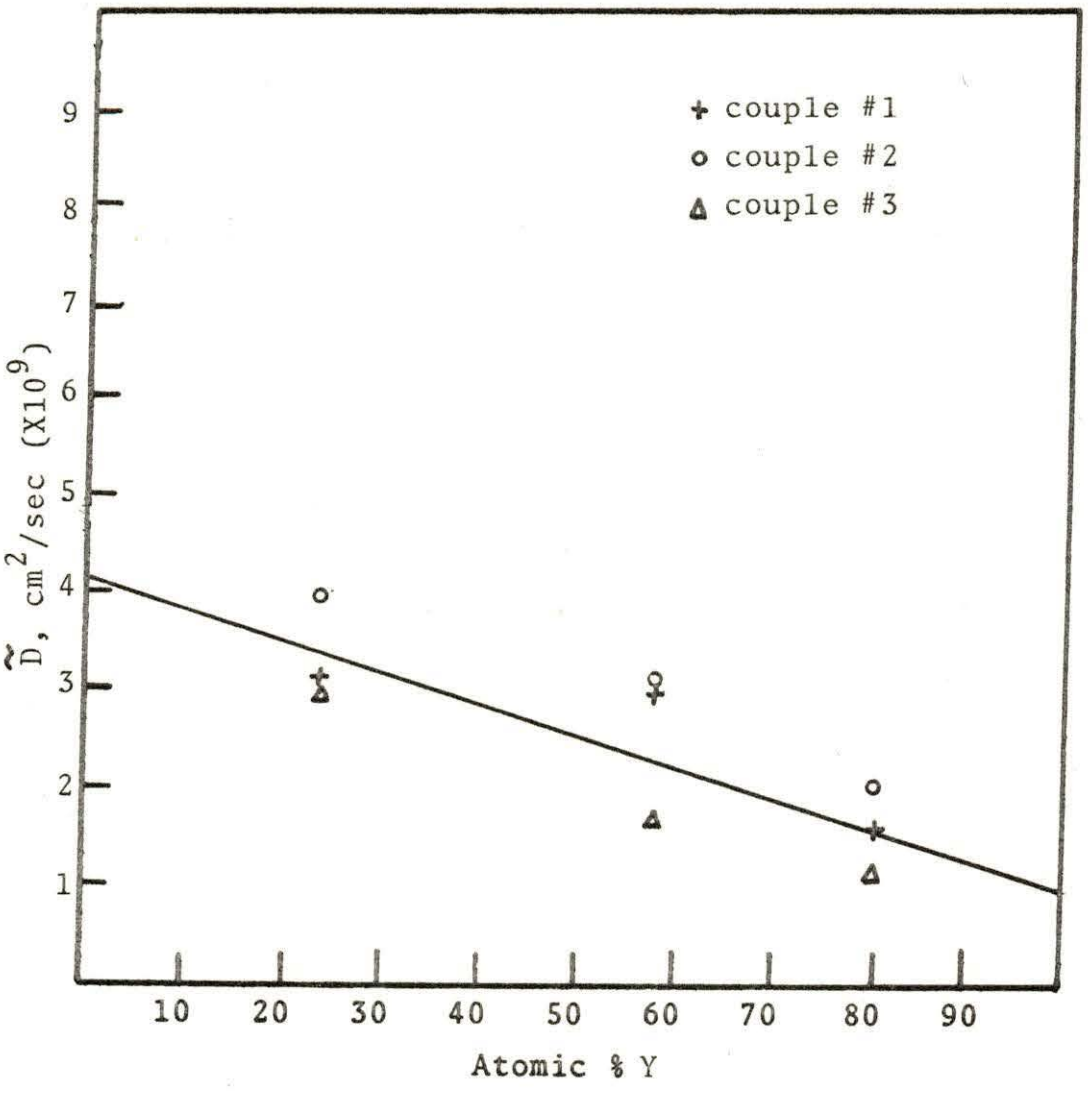

Figure 28. Er_2O_3-Y_2O_3, 1890°C, 2 hr 15 min

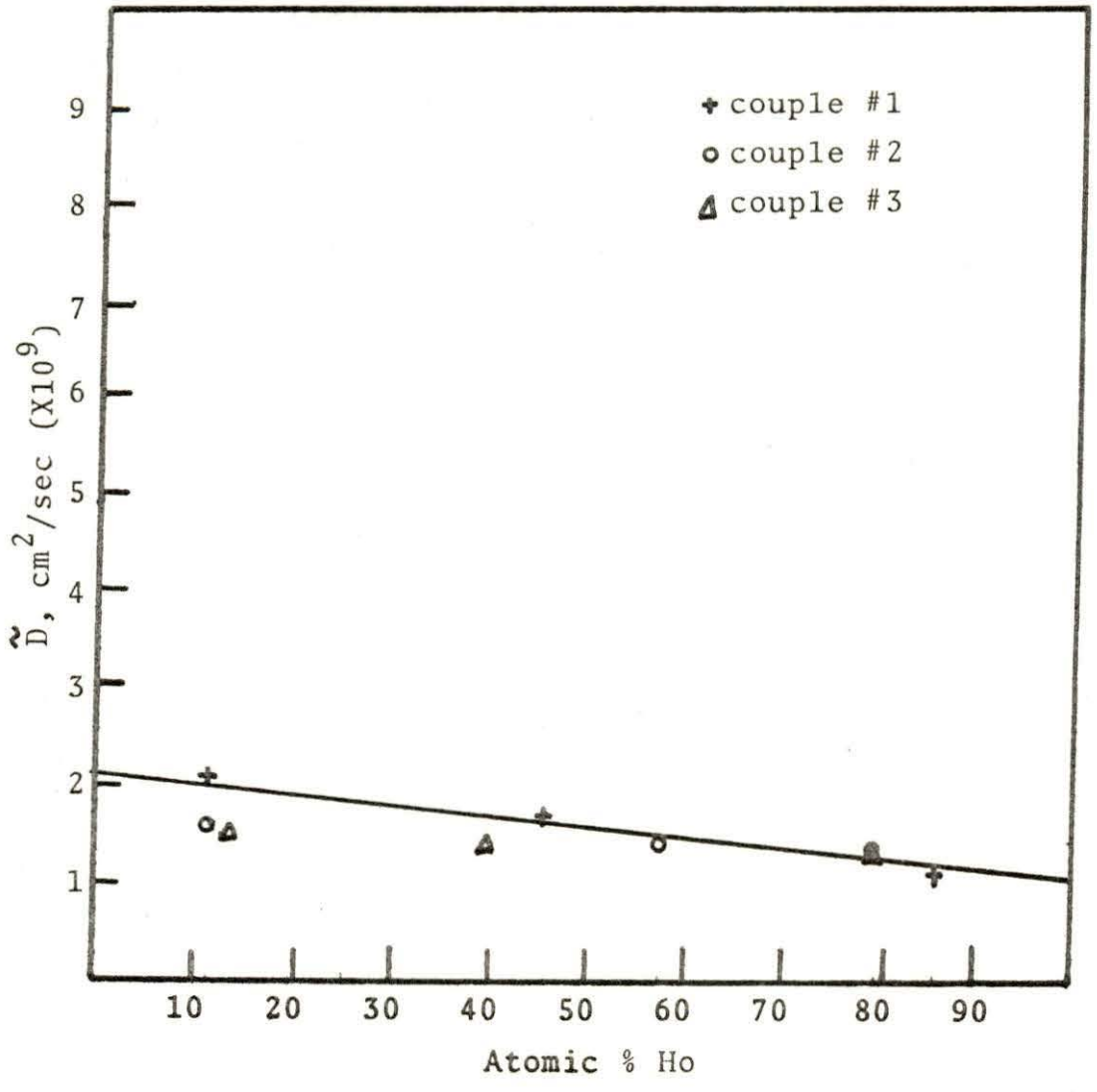

Figure 29. Er_2O_3-Ho_2O_3, 1890°C, 2 hr 15 min

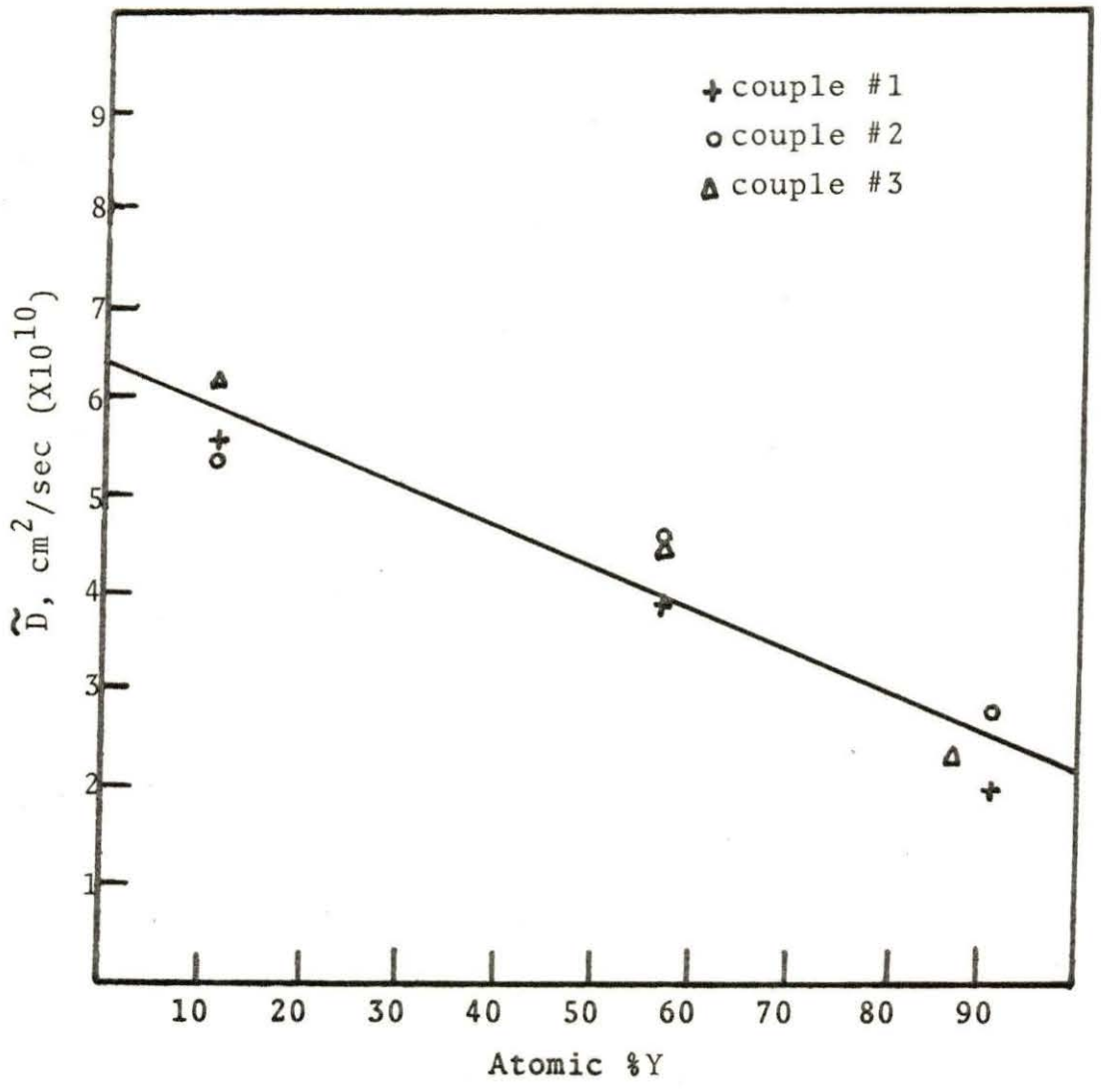

Figure 32. Er_2O_3-Y_2O_3, 1700°C, 16 hr

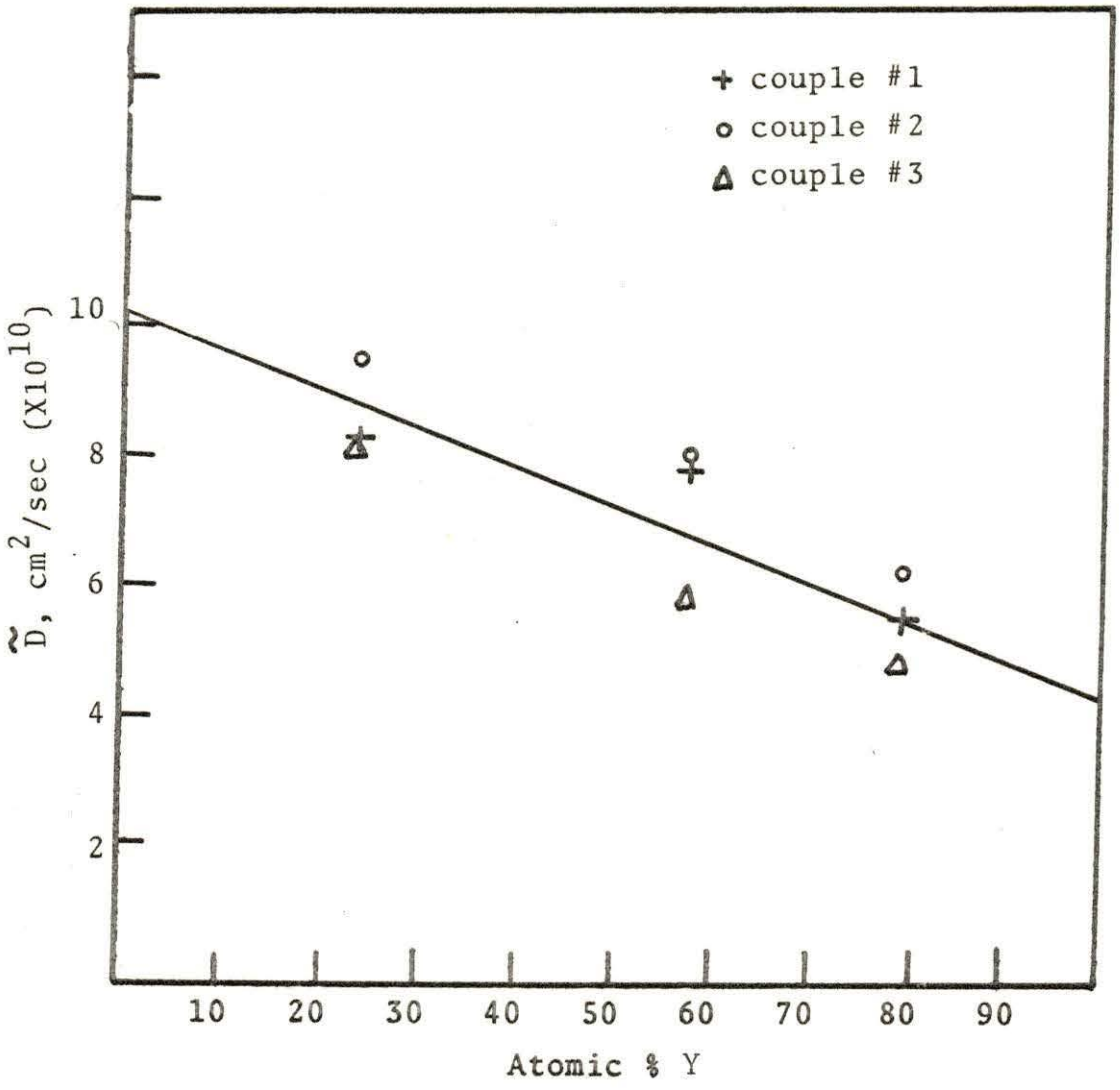

Figure 30. Er_2O_3-Y_2O_3, 1780°C, 10 hrs

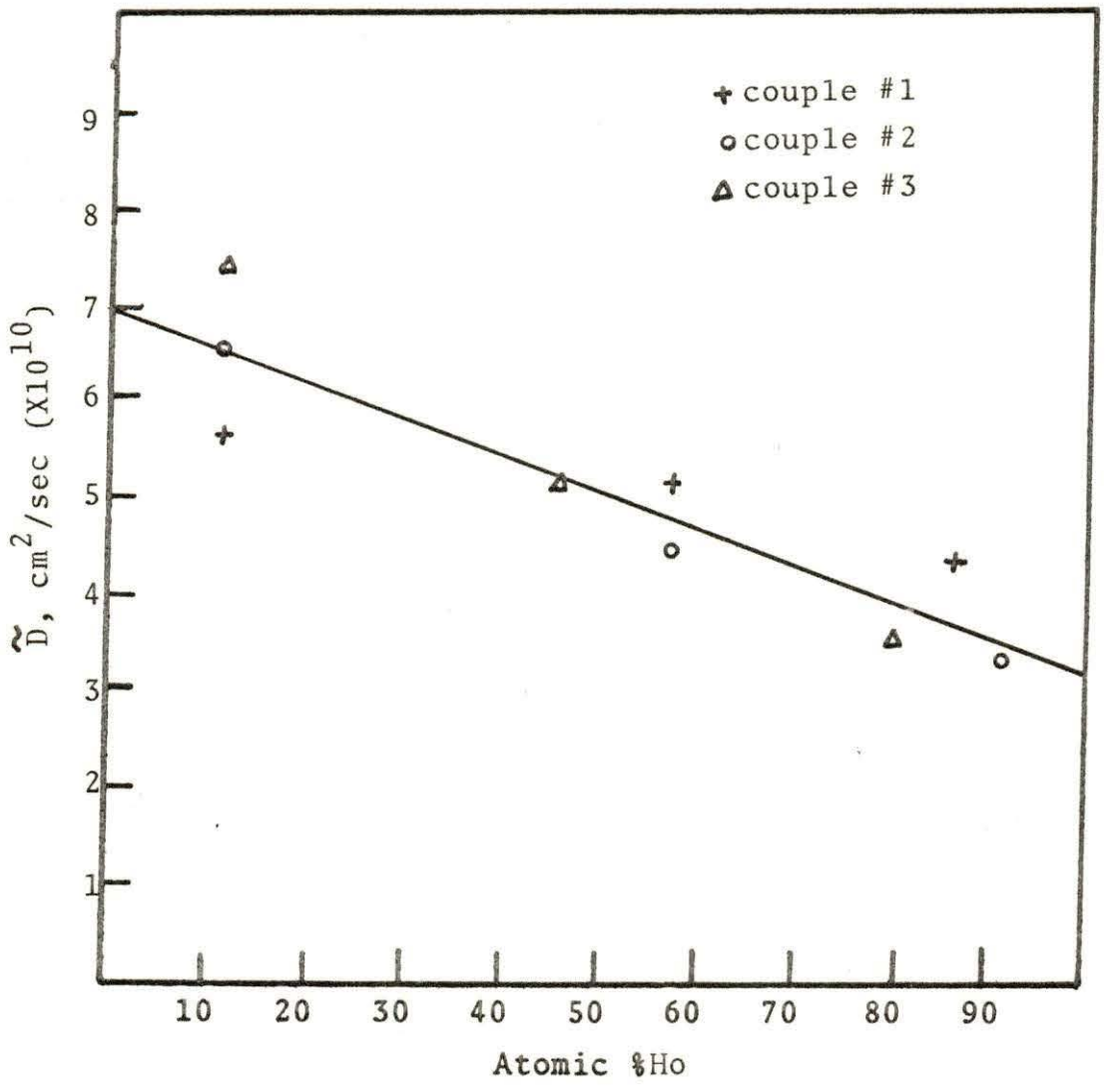

Figure 31. Er_2O_3-Ho_2O_3, 1780°C, 10 hr

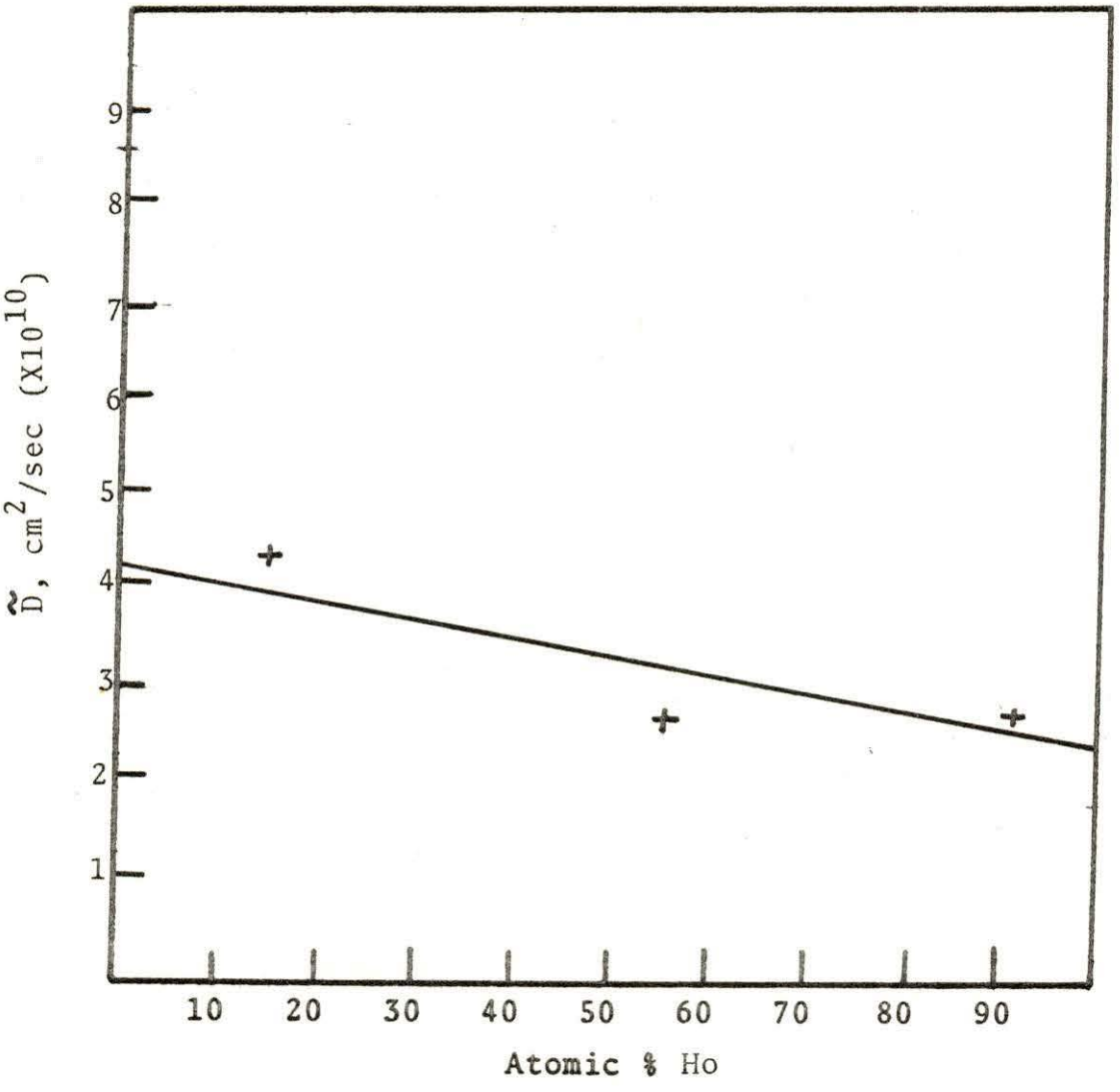

Figure 33. Er_2O_3-Ho_2O_3,,1700°C, 16 hrs

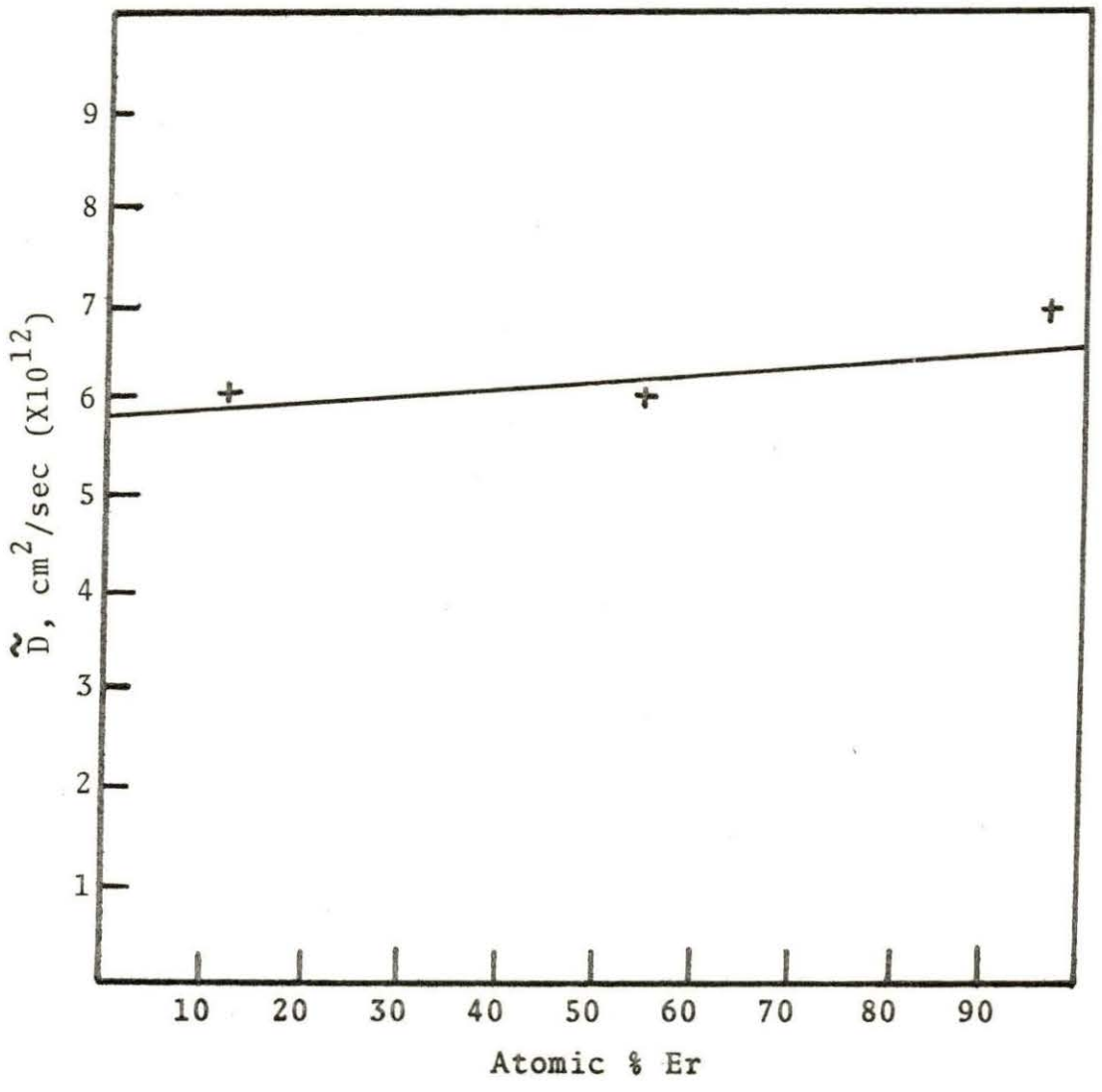

Figure 34. Er_2O_3-Y_2O_3, 1400°C, 23 days 14 hr 40 min

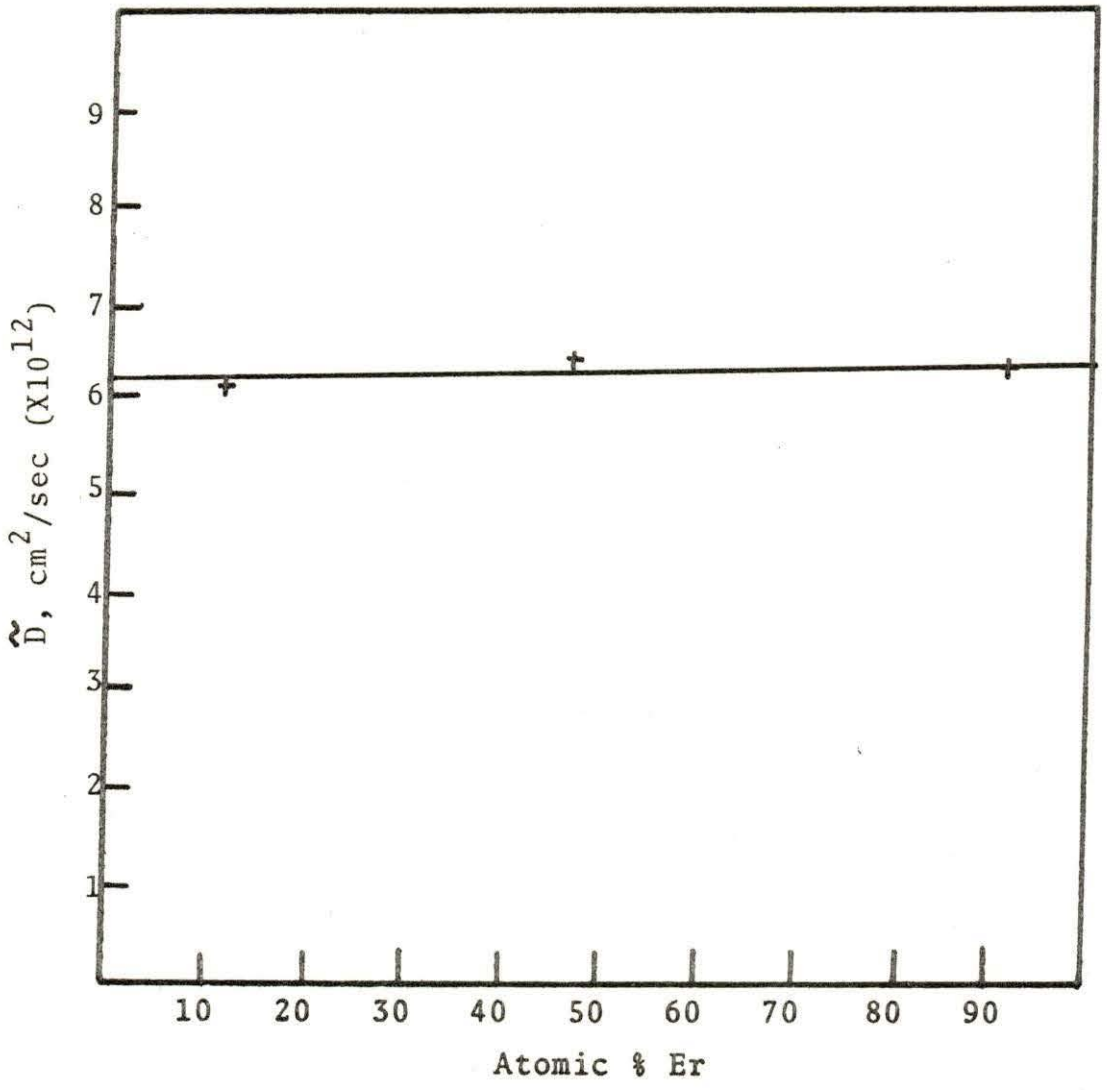

Figure 35. Er_2O_3-Ho_2O_3, 1400°C, 23 day, 14 hr, 40 min

Table 2. Constants "m" and "b" for the equation $\tilde{D} = mc + b$

Temperature (°C)	Couple	Slope "m" $(cm^2/sec)/atom\%$	Intercept "b" (cm^2/sec)
1890	Y_2O_3-Er_2O_3	-0.03182	4.182×10^{-9}
1890	Ho_2O_3-$Er_2)_3$	-0.01027	2.125×10^{-9}
1780	H_2O_3-Er_2O_3	-0.05773	1.021×10^{-9}
1780	Ho_2O_3-Er_2O_3	-0.03760	6.950×10^{-10}
1700	Y_2O_3-Er_2O_3	-0.04232	6.417×10^{-10}
1700	Ho_2O_3-Er_2O_3	-0.02762	4.003×10^{-10}
1400	Y_2O_3-Er_2O_3	-0.007631	6.5831×10^{-10}
1400	Ho_2O_3-Er_2O_3	-0.001190	6.390×10^{-12}

The experimentally observed linearity of the data, is as expected on physical ground due to the similarity of Y, Ho and Er ions (in valence, size, chemical properties but not in mass). It should be noted that due to experimental difficulties, only one set of data points was obtained at 1400°C for both the Ho_2O_3-Er_2O_3 and Y_2O_3-Er_2O_3 systems and at 1700°C for the Ho_2O_3-Er_2O_3 system. These points are thus less well determined.

Comparison of values for $\tilde{D}$ in both systems at a given temperature reveals a higher interdiffusion coefficient in the Y_2O_3-Er_2O_3 than in the Ho_2O_3-Er_2O_3 system. As composition tends toward 0% Er_2O_3, the values of $\tilde{D}$ corresponding to the

two systems approach a single value.

It will be recalled that one of the objectives of this work was to describe the data by means of an Arrhenius expression.

$$\tilde{D} = \tilde{D}_o \, e^{-Q/RT}$$

where $\tilde{D}$ - interdiffusion coefficient

Q - activation energy

$\tilde{D}_o$ - fundamental constant (vibrational term)

Figures 36 through 42 present Arrhenius plots for the systems at various compositions. Table 3 provides a summary of the values of $\tilde{D}_o$ and Q corresponding to selected concentration. Values of $\tilde{D}$ obtained by using the tabulated constants should be rounded off to at most three significant figures.

In obtaining the fits, points at 1400°C were not included because of the observed presence of intergranular cracking in these hot pressed specimens. It should be made clear that at all other temperatures, anneals were made on isostatically-pressed and sintered material. Intergranular cracking in the hot-pressed material could account for a higher than expected value for $\tilde{D}$ at 1400°C. The effect would be probably due to the introduction of porosity.

The general trends in activation energy, Q and $\tilde{D}_o$ with composition variation are shown by the entries in Table 3. It should be noted that the variations in activation energy

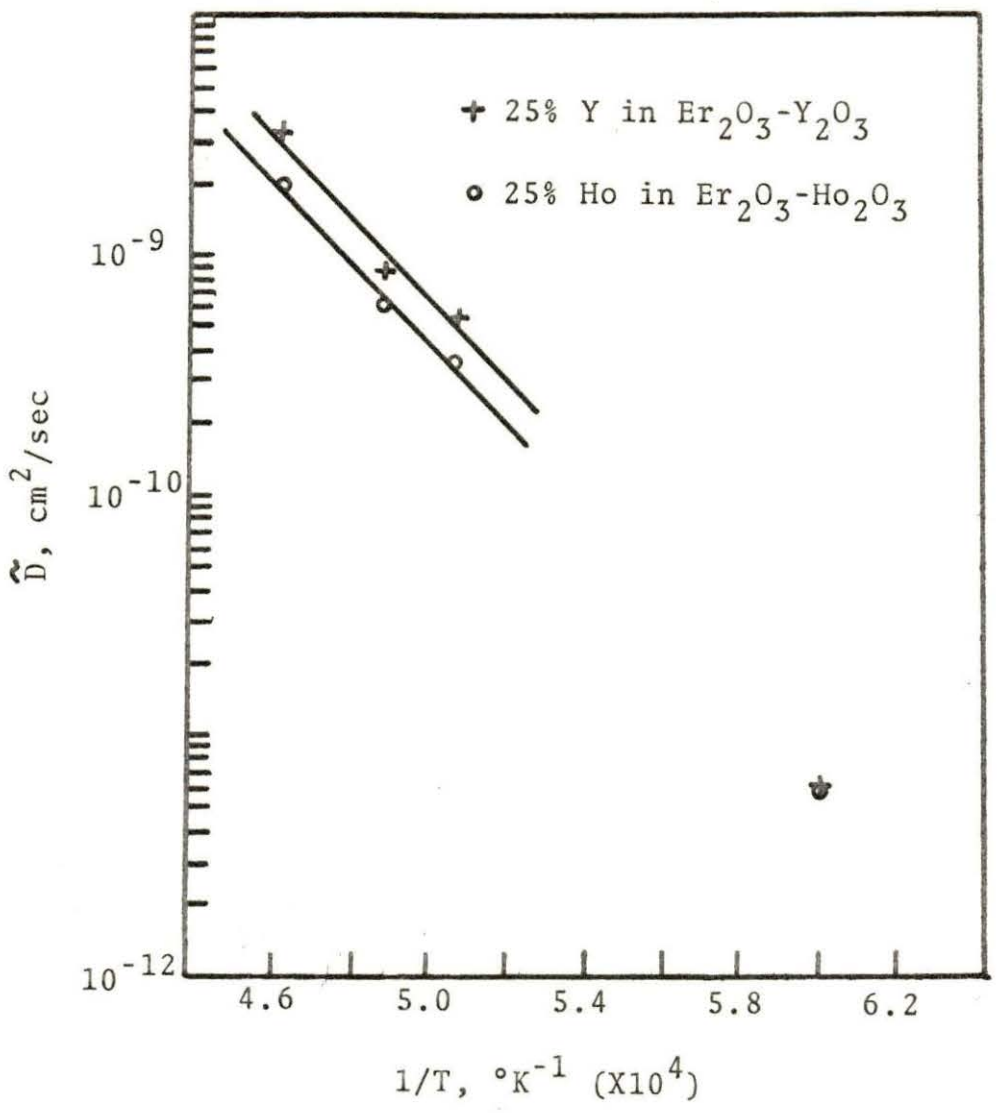

Figure 36. Arrhenius plot of interdiffusion coefficient

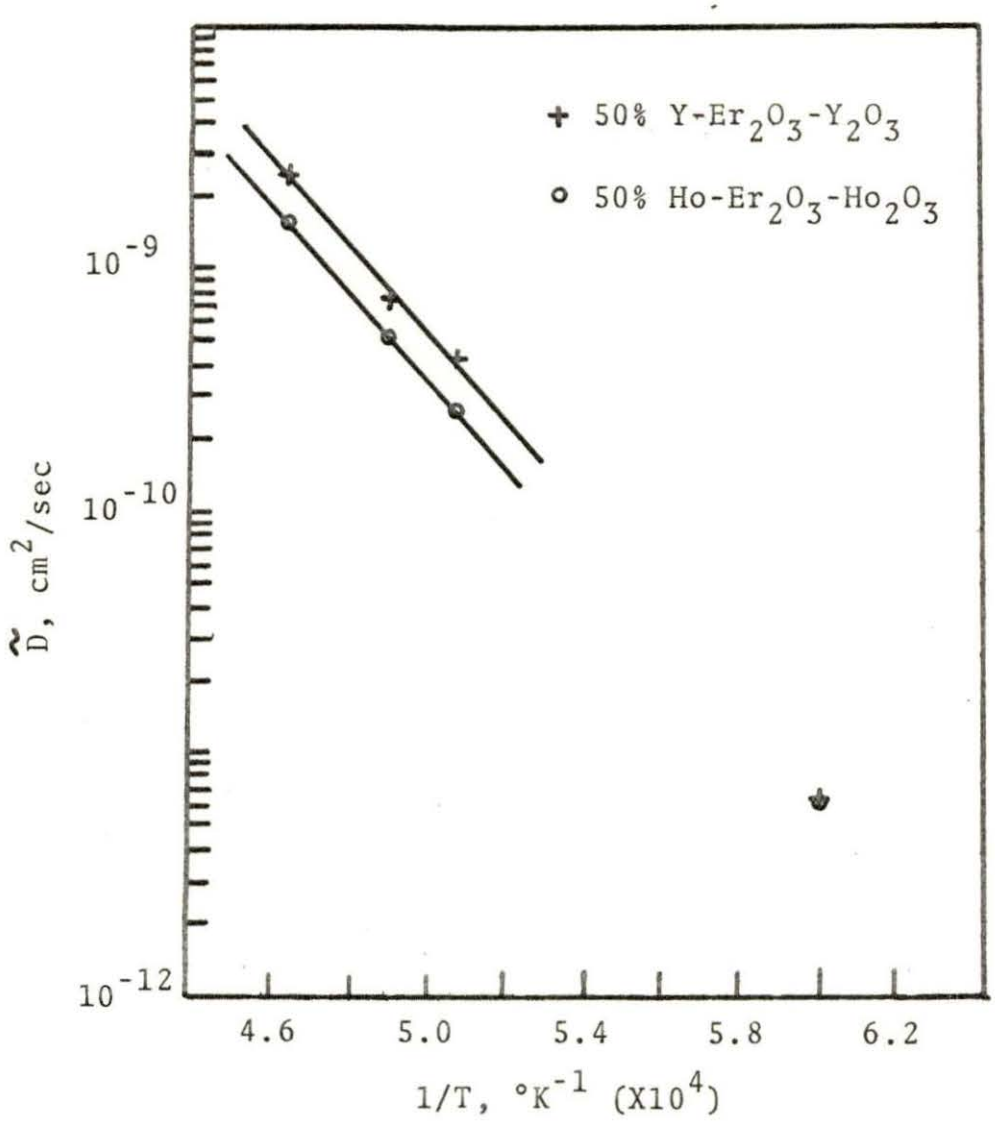

Figure 37. Arrhenius plot of interdiffusion coefficient

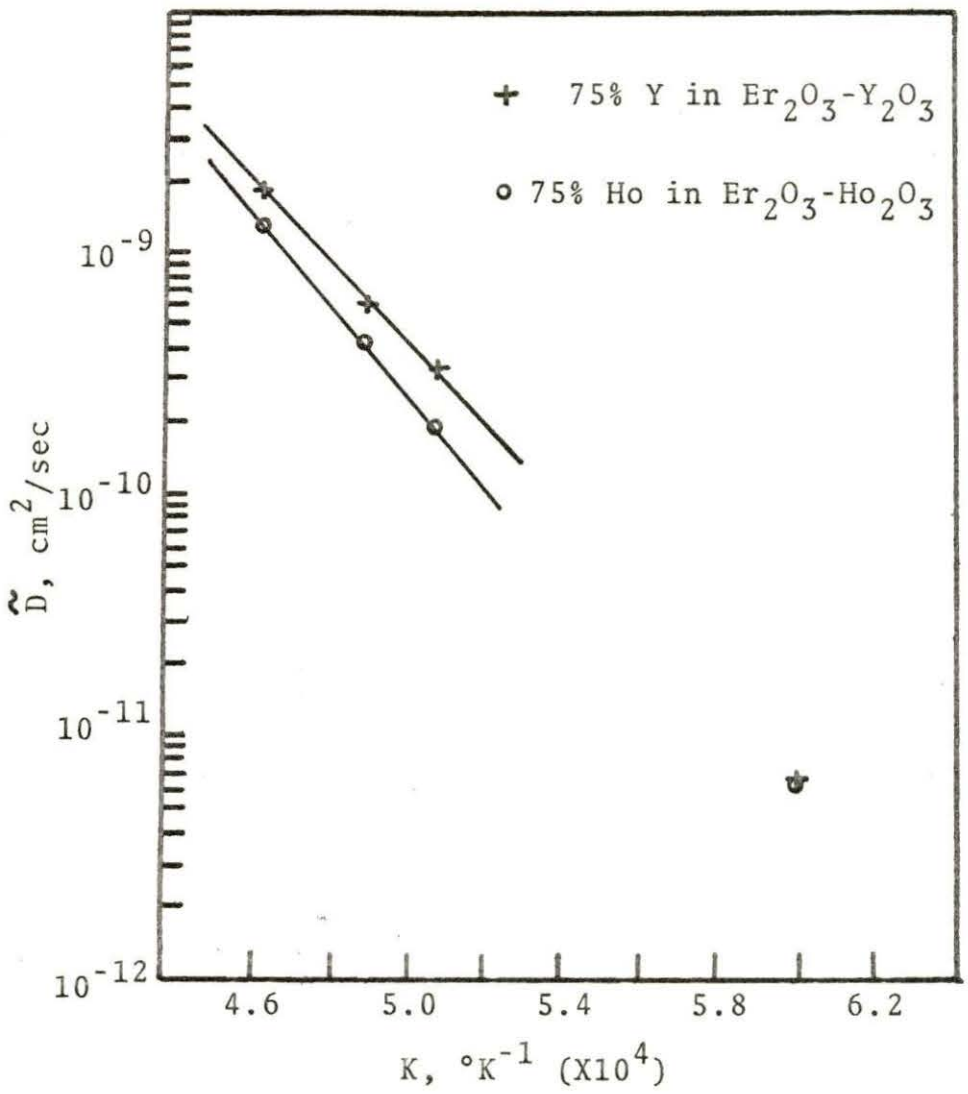

Figure 38. Arrhenius plot of interdiffusion coefficient

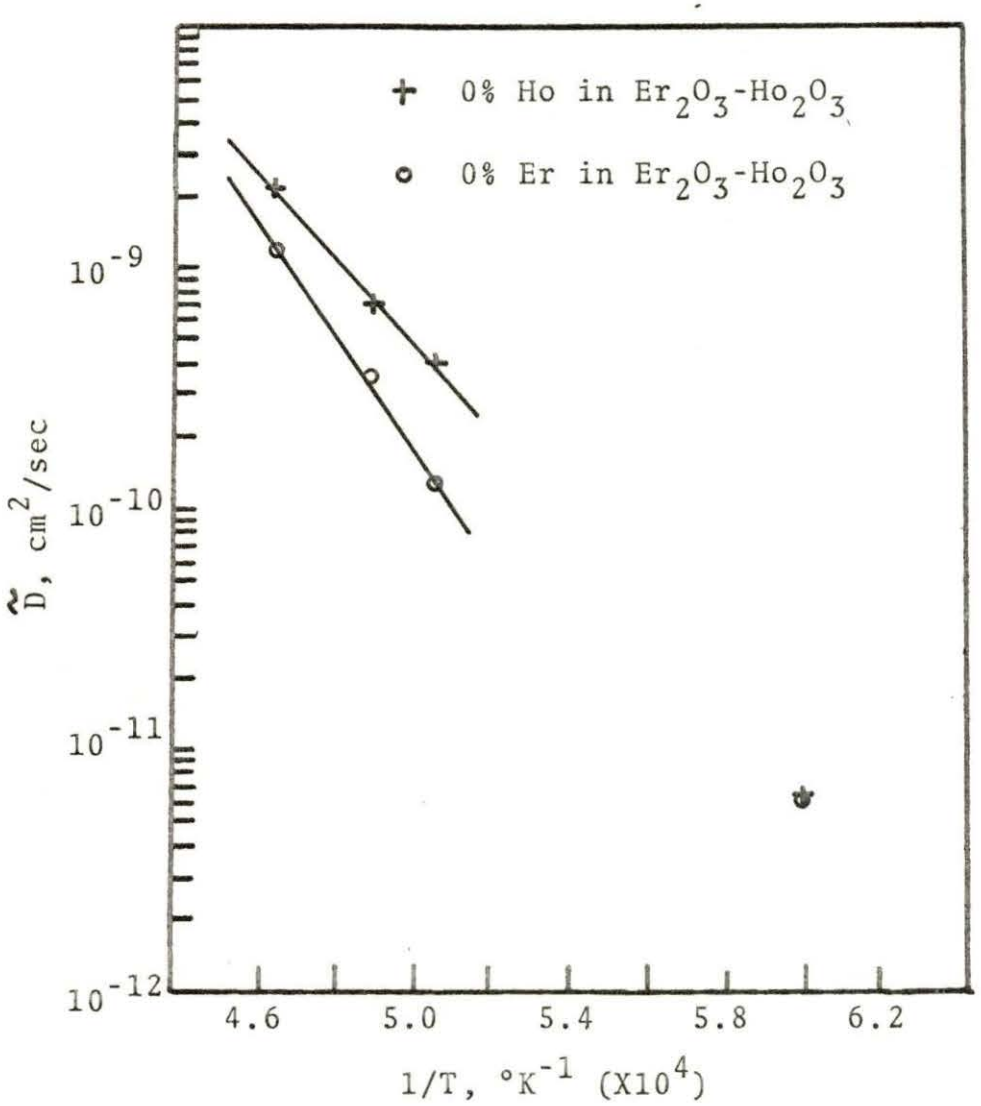

Figure 39. Arrhenius plot of interdiffusion coefficient

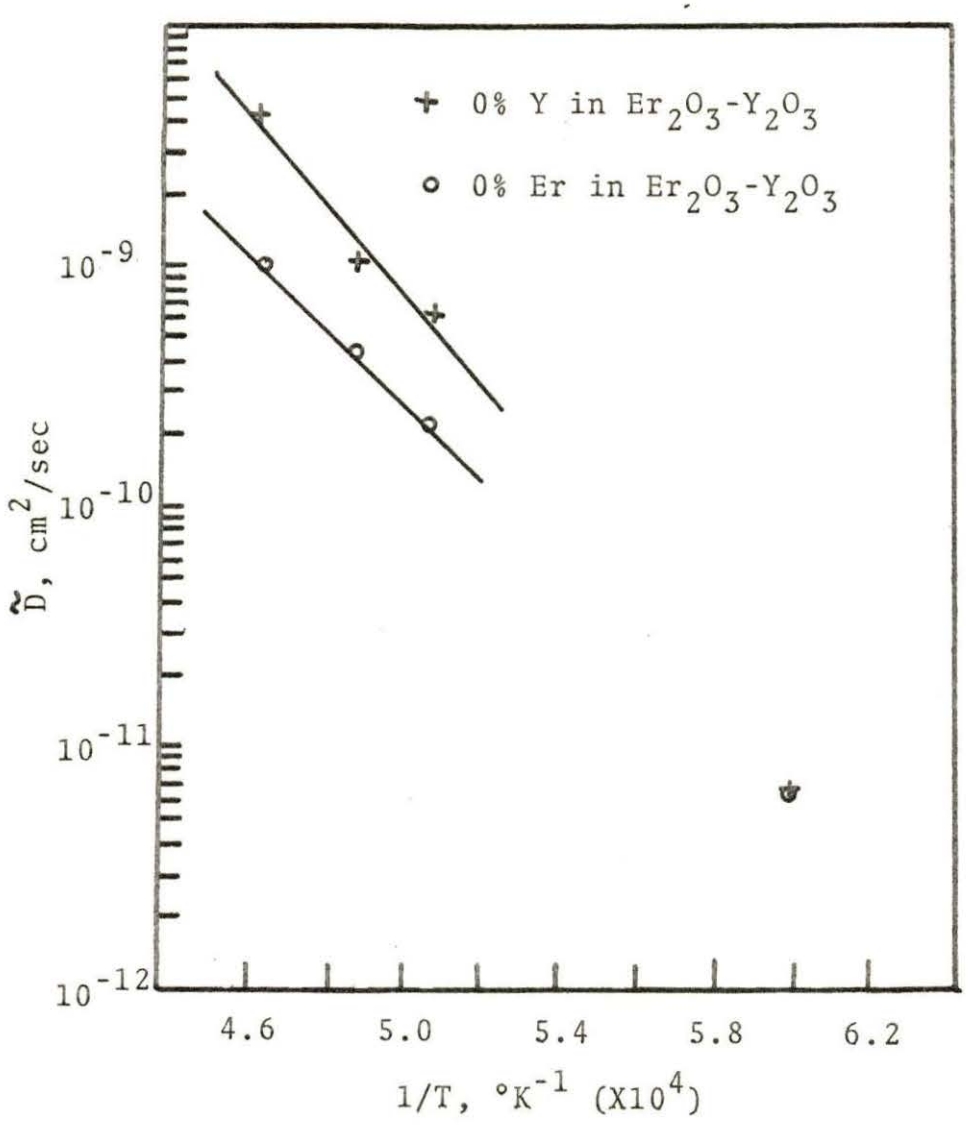

Figure 40. Arrhenius plot of interdiffusion coefficient

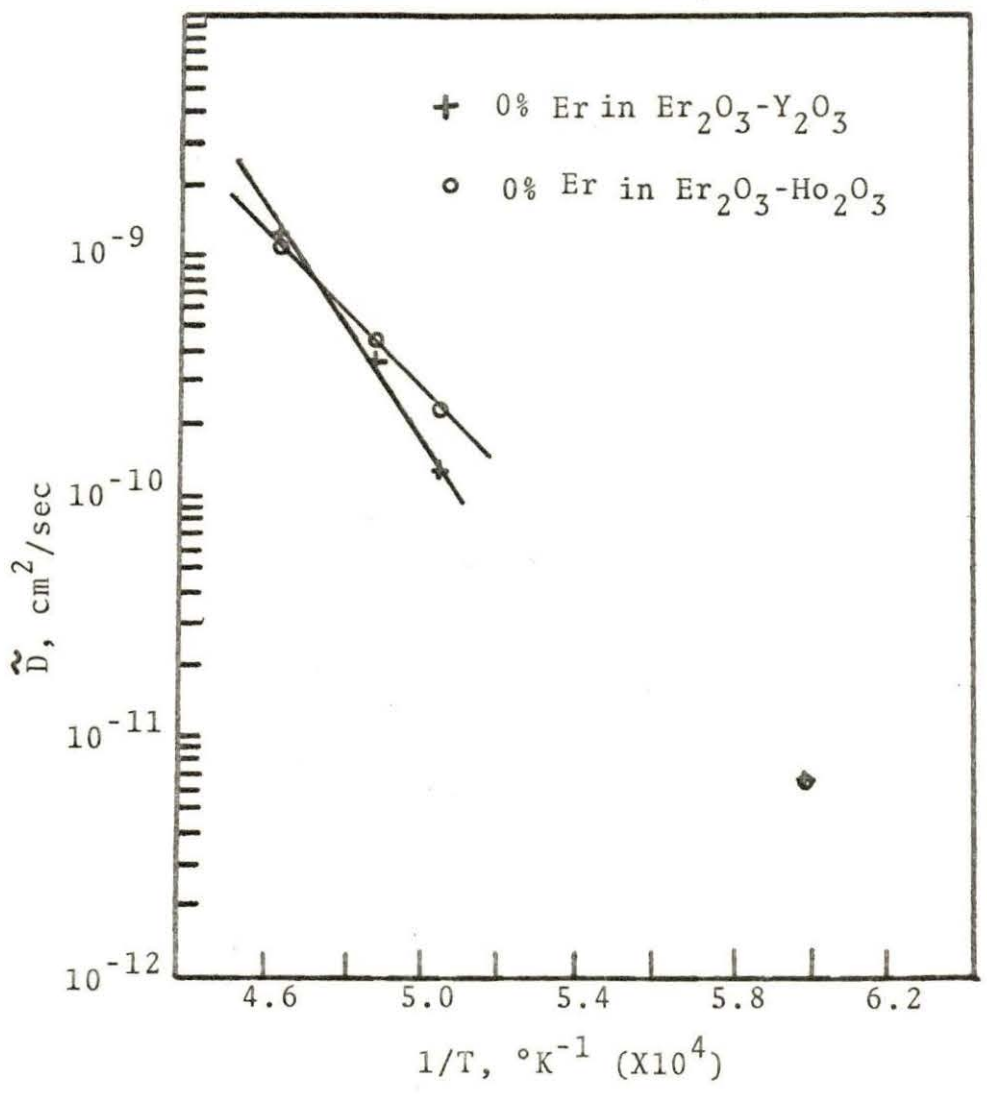

Figure 41. Arrhenius plot of interdiffusion coefficient

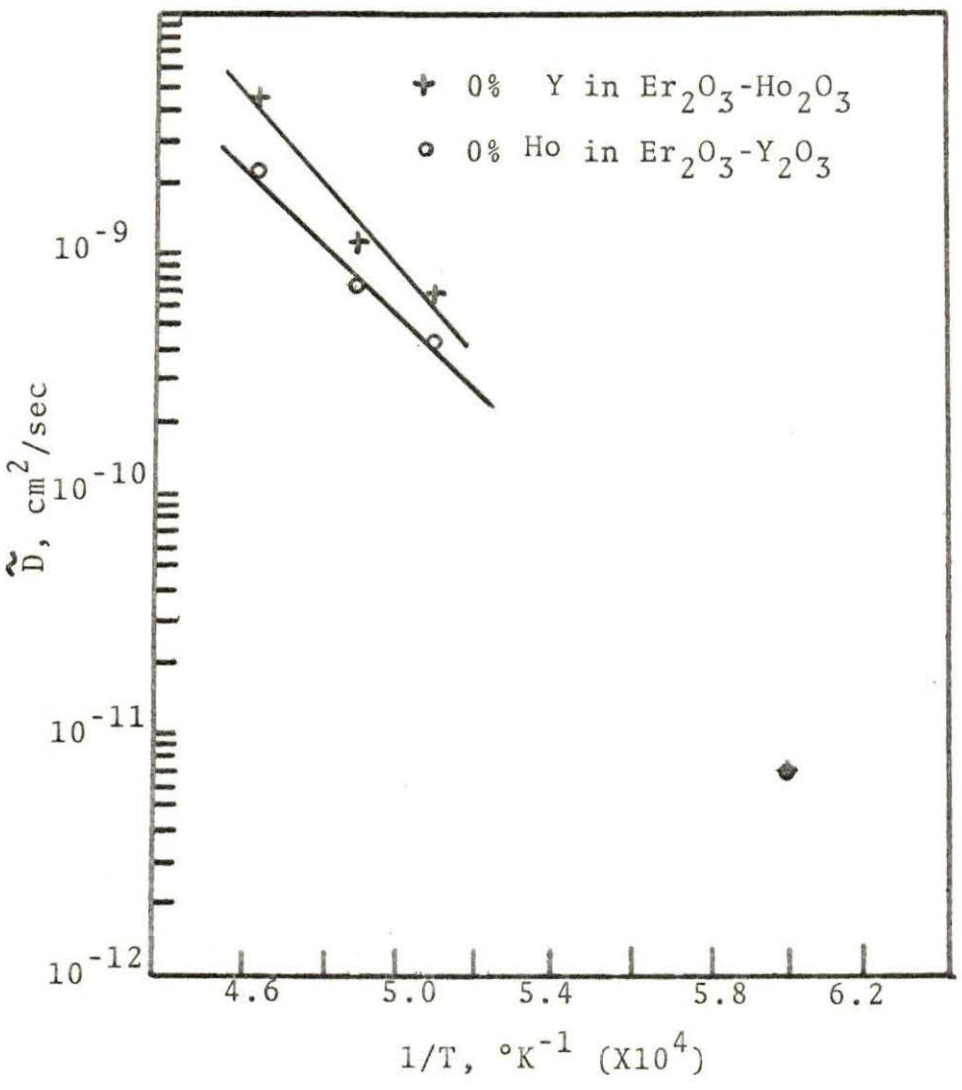

Figure 42. Arrhenius plot of interdiffusion coefficient

Table 3. Fitted constants for the Arrhenius equation $\tilde{D} = \tilde{D}_o e^{-Q/RT}$

Composition	System	D_o cm^2/sec	Q(cal/mole)
0% Er	Y_2O_3-Er_2O_3	6.368×10^{-3}	67,110
0% Y	Y_2O_3-Er_2O_3	1.246×10^{0}	84,098
0% Er	Ho_2O_3-Er_2O_3	6.310×10^{0}	96,356
0% Ho	Ho_2O_3-Er_2O_3	6.982×10^{-2}	74,425
75% Y	Y_2O_3-Er_2O_3	9.022×10^{-2}	76,213
75% Ho	Ho_2O_3-Er_2O_3	7.464×10^{-1}	86,413
50% Y	Y_2O_3-Er_2O_3	3.266×10^{-1}	80,202
50% Ho	Ho_2O_3-Er_2O_3	2.340×10^{-1}	80,741
25% Y	Y_2O_3-Er_2O_3	7.204×10^{-1}	82,601
25% Ho	Ho_2O_3-Er_2O_3	1.138×10^{-1}	77,049

are larger than would be expected from classical theory. One would expect no variation since activation energy is mass independent, and the ions Ho, Y, Er are very similar in every respect (even size) except mass. Thus the variations in the values of Q measured at 25%, 50% and 75% composition reflect overall experimental uncertainties rather than expected variations. Similarly, although values of $\tilde{D}_o$ reflect the expected dependence on mass, little significance should be attached to their exact values. The trend at most c values is a decrease in $\tilde{D}_o$ from Y (mass = 89) to H_o (mass = 165) to

Er (mass = 167) which is fairly consistent with the expectation that a less massive ion should have less inertia and consequently a higher vibration rate. The numerical values of $\tilde{D}_o$, since they are obtained from extrapolations far beyond the experimental data, may have a relatively large associated uncertainty.

Figures 39 and 40 give the results of extrapolation of the $\tilde{D}$ vs C plots to 0% Er, 0% Y and 0% Er, 0% Ho respectively. These can be regarded as approximations to impurity diffusion coefficients of Er in Y_2O_3, Y in Er_2O_3, Er in Ho_2O_3 and Ho in Er_2O_3. Darken's Equation 19 will help to explain why an interdiffusion coefficient can be decomposed into two separate intrinsic diffusion coefficients.

$$\tilde{D} = N_2D_1 + N_1D_2 \qquad (23)$$

$\tilde{D}$ - interdiffusion coefficient

N_1, N_2 - mole fractions

D_1, D_2 - intrinsic diffusion coefficients

The equivalence of an intrinsic diffusion coefficient with an impurity diffusion coefficient requires that no Kirkandall effect be present. No such effect is indicated in these systems thus the two coefficients are set equal. One then reasons that at $N_2 = 0$ for example, there is little difference in D and the diffusion coefficient D_2.

Figures 41 and 42 permit a comparison of impurity dif-

fusion coefficients of both Y and Ho in Er_2O_3, and Er in both Y_2O_3 and Ho_2O_3 respectively. From Figure 42 one can see only a slight difference (probably due to experimental error) of impurity Er diffusion in both Y_2O_3 and Ho_2O_3. This is expected due to the fact that the Y_2O_3 and Ho_2O_3 matrixes are so similar. Here both pairs of values of $\tilde{D}_o$ and Q are the same as expected. One point (from 1700°C Ho_2O_3-Er_2O_3 couple) deviates widely but since it is derived from a limited amount of data (only three data points rather than the nine which define the other points) a greater uncertainty is expected.

Figure 41 presents data of Ho impurity diffusion coefficients in Er_2O_3 and Y impurity diffusion coefficients in Er_2O_3. As expected, little variation in activation energy is observed while the less massive Y ion is seen to have higher values of $\tilde{D}_o$.

CONCLUSIONS

1. The predictions of classical diffusion theory are upheld in the systems Y_2O_3-Er_2O_3 and Ho_2O_3-Er_2O_3. An independence of the activation energy Q, with mass and a decrease in $\tilde{D}_o$ with mass increase, are observed.

2. The defective anion lattice of the C-cubic fluorite structured rare earth oxides is capable of accommodating the Ar atom.

3. Interdiffusion coefficients and impurity diffusion coefficients variation with temperature and concentration have been measured and the results reduce to equations whose parameters are presented in Tables 2 and 3.

4. The procedures explored in this study for the preparation of hot pressed rare-earth oxides are not suitable for diffusion studies due to the fact that the product displays a density variation resulting from intergranular cracking.

5. Rare-earth oxide "bloating" is prevented by outgassing at 1400°C.

6. The overall results of the experiments have not revealed any characteristics which would detract from the potential usefulness of rare earth oxides for nuclear reactor control poisons.

SUGGESTIONS FOR FURTHER WORK

(1) A systematic investigation of the bloating phenomena in rare-earth oxides is needed. This study should be guided toward the explanation of the cause rather than a mere elimination of its result.

(2) An examination of the rod-like structures to determine if a preferred direction of crystal growth is present could also be of value. This work should begin with an electron diffraction analysis of the rods to determine their structure.

(3) Work on obtaining high density rare-earth oxides, by use of metal-organic active powders, could improve specimen density and reduce grain size by allowing for lower sintering temperatures.

(4) Investigation of an observed reaction product between the rare-earths and Pt-Rh alloys at temperatures 1700°C and 1800°C could also be done.

(5) More detailed study on dissolution of gases in rare-earth oxides would provide additional data on these materials.

(6) Comparison of the sectioning technique and microprobe analysis method for diffusion coefficient measurement needs to be done. For this study the experimenter has supplied several diffusion couples that "fell apart"

(7) During an early anneal done in an induction furnace the specimens and crucibles were converted into a fibrous

mass. This fiber could possibly be of technological value and has been given to others for an X-ray analysis.

BIBLIOGRAPHY

1. MARC FOEX AND JEAN-PIERRE, Revue International des Hautes Temperatures et des Refractaires 3, 429 (1966).

2. M. F. BERARD, "Diffusion in Polycrystalline Y_2O_3 and Er_2O_3," Ph.D. Dissertation, Iowa State University (1968).

3. F. E. JAUMOT, JR., "A Bibliography of Diffusion of Gases, Liquids, and Solids in Solids, 1890 to 1955," U.S. Atomic Energy Commission Report TID-3071 (Division of Technical Information Extension, AEC) (1958).

4. MICHAEL F. BERARD, "Diffusion in Ceramic Systems; a Selected Bibliography," U.S. Atomic Energy Commission Report IS-448 (Iowa State University of Science and Technology, Ames Inst. for Atomic Research) (1962).

5. J. LOMMEL, "Literature Survey on the Diffusion of Metals into Oxides," U.S. Atomic Energy Commission Report AD-75227 (Defense Documentation Center) (1954).

6. R. LINDER, Z. Naturforschung, 10A 1027-1028 (1958).

7. P. A. CUMMING AND P. J. HARROP, "Bibliographic Review of Self-diffusion in Metal Oxides," U.S. Atomic Energy Commission Report AERE-Bib. 143 (Gt. Brit. Atomic Energy Commission Establishment, Harwell, Berks, England) (1965).

8. JOHN ASKILL, Tracer Diffusion for Metals, Plenum Publishing Corp., New York (1970).

9. ALLEN M. ALPER, High Temperature Oxides, Academic Press, New York (1970).

10. DIFFUSION INFORMATION CENTER, Diffusion Data, Vol. 1, Diffusion Information Center, Cleveland, Ohio (1967).

11. J. CRANK, The Mathematics of Diffusion, The Clarendon Press, Oxford, England (1957).

12. W. JOST, Diffusion in Solids, Liquids, Gases, Academic Press, Inc., New York (1952).

13. DAVID A. FRANK-KAMENETSKII, Diffusion and Heat Transfer in Chemical Kinetics, Plenum Press, New York (1969).

14. R. M. BARRER, Diffusion in and through Solids, University Press, Cambridge, England (1941).

15. PAUL G. SHEWMON, Diffusion in Solids, McGraw-Hill Book Co., New York (1963).

16. L. A. GIRIFALCO, Atomic Migration in Crystals, Blaisdell, New York (1964).

17. Y. ADDA AND J. PHILIBERT, La Diffusion dans les Solides, Institute National Des Sciences et Techniques Nuclearies, Saclay, France (1966).

18. AMERICAN SOCIETY FOR METALS, Diffusion in Body-Centered Cubic Metals, American Society for Metals, Cleveland, Ohio (1965).

19. AMERICAN SOCIETY FOR METALS, Atom Movements, American Society for Metals, Cleveland, Ohio (1951).

20. R. F. MEHL, Trans. Am. Inst. Mining Met. Engrs. 122, 11-56 (1936).

21. R. L. ANDELIN AND L. E. GODFREY, "Bibliography on Self-diffusion of Pure Metals in the Solid State, U.S. Atomic Energy Commission Report LAMS-2562 [Los Alamos Scientific Laboratory, New Mexico] (1961).

22. V. N. SVECHNIKOV, Metallofizka, 25 (1968).

23. E. A. GIESS, Diffusion and Conduction in Ionic Solids, State University of New York College of Ceramics, Alfred University, Alfred, New York (1958).

24. P. SUPTITZ AND J. TELTOW, Physica Status Solidi, 23, 9-56 (1967).

25. HERBERT HERMAN, Advances in Materials Research, 4, John Wiley and Sons, Inc., New York (1970).

26. C. E. BIRCHENALL, "Diffusion in Oxides; Assessment of Existing Data and Experimental Problems," U.S. Atomic Energy Commission Report UCRL-70715 [Lawrence Radiation Lab.] (1967).

27. CENTRE D'ETUDES NUCLEAIRES DE SACLAY, Colloque sur la Diffusion a l'Etate Solide, Center d'Etudes Nucleaires de Saclay, Saclay, France (1959).

28. J. B. WACHTMAN AND A. D. FRANKLIN, Eds., Mass Transport in Oxides, National Bureau of Standards, Special Publication 296 (1968).

29. M. F. BERARD, "Self-diffusion in Polycrystalline Yttrium Oxide," M.S. thesis, Iowa State University (1962).

30. A. ASCOLI AND E. GERMAGNOLI, Pure and Applied Chemistry 1, 139-141 (1960).

31. R. M. CONANT, "Measurement of Interdiffusion in the System Mn_xO-MgO by Neutron Activation Analysis, M.S. thesis, Iowa State University (1970).

32. A. I. KOIFMAN AND O. R. NIYAZOVA, Fiz. Tekh. Polvprovodn 3, 1405-6 (1969).

33. A. E. KIV AND F. T. UMAROVA, Soviet Physics-Solid State 8, 1745-1749 (1968).

34. THEODOR HEHENKAMP, J. Applied Phys., 39 , 3928-30 (1968).

35. C. M. WALTER, "Review of Status of Self-diffusion in US, UN, UO_2 and UC," U.S. Atomic Energy Commission Report ANL-7094 [Argonne National Lab.] (1965).

36. A. N. ASHURST, Reactor Materials, 12, 25-59 (1969).

37. M. F. BERARD, C. D. WIRKUS AND D. R. WILDER, J. Am. Ceramic Soc. 51, 643 (1968).

38. K. M. MINACHEV AND G. V. ANTOSHIN, Dokl. Akad. Nauk. SSSR 161, 122 (1966).

39. L. A. SAZONOV, A. N. RATOV, AND T. G. RATOV, Kinet. Kataliz 6, 836 (1965).

40. G. D. STONE, "Self-diffusion of Oxygen in Neodymium and Samarium Sesquioxide," Ph.D. Dissertation, Arizona State University, Tempe, Arizona (1968).

41. I. V. VINOKUROV, Izv. Akad. Nauk SSSR Neorgn. Mater., 6, 328-33 (1970).

42. C. D. WIRKUS, M. F. BERARD, AND D. R. WILDER, J. Am. Ceram. Soc. 52, 456 (1969).

43. H. J. SVEC AND T. J. RIDER, J. Less Common Metals 14, 103-12 (1968).

44. A. FICK, Prog. Ann., 94, 59 (1855). Original not available; cited in J. Crank, Mathematics of Diffusion, p. 2, The Claredon Press, Oxford, England (1957).

45. J. B. FOURIER, Oeuvres de Fourier (1822). Original not available; cited in J. Crank, Mathematics of Diffusion, p. 2, The Claredon Press, Oxford, England (1957).

46. L. W. BARR AND A. D. LeCLAIRE, Proc. Brit. Ceram. Soc., 1, 190 (1964).

47. CLARENCE ZENER, J. Applied Physics, 22 , 372 (1951).

48. C. A. WERT, J. Applied Physics 20, 943 (1949).

49. SAMULE GLASSTONE, KEITH J. LAIDIER AND HENRY EYRING, The Theory of Rate Processes, McGraw-Hill Book Co., New York (1941).

50. JOHN MANNING, Diffusion Kinetics for Atoms in Crystals, D. Van Nostrand Co., Inc., Princeton, New Jersey (1968).

51. C. ZENER, in Imperfections in Nearly Perfect Crystals, W. Shockley, J. H. Hollomon, R. Maurer and F. Sertz, Eds., pp. 289-314, John Wiley and Sons, Inc., New York (1952).

52. R. S. ROTH AND S. J. SCHNEIDER, "F. Research National Bureau of Standards," 64A, No. 4, 309 (1960).

53. M. OMINI, Nova Cimento, LIVB 116 (1968).

54. J. C. FISHER, J. Applied Physics, 22 , 74 (1951).

55. R. T. P. WHIPPLE, Phil. Mag., 45, 1225 (1954).

56. T. SUZUOKA, J. Phys. Soc. Japan, 19, 839 (1964).

57. R. F. CANON AND J. P. STARK, J. Applied Physics, 40, 4361-6 (1969).

58. GEORGE KUCZYNSKI, Bull. Soc. Fr. Ceram., 80 , 45-52 (1968).

59. C. A. PAMPILLO AND N. W. DERECA, J. Mat. Sci. 4, 985-8 (1969).

60. J. MIMKES AND M. WUTTIG, J. Appl. Phys. 41, 3205-9 (1970).

61. B. J. WUENSCH AND T. VASILOS, J. Am. Ceram. Soc., 49, 433 (1968).

62. A. J. MORTLOCK, J. Aust. Inst. for Metals 14, 98-101 (1969).

64. JOHN J. BURKE, NORMAN L. REED AND VOLKER WEISS, Surfaces and Interfaces I - Chemical and Physical Characteristics, Syracuse University Press, Syracuse, New York (1967).

65. C. A. WERT, Phys. Rev., 79 601 (1950).

66. P. G. SHEWMON AND J. Y. CHOI, Trans. A.I.M.E., 230, 123 (1964).

67. P. WYNBLATT AND N. A. GJOSTEIN, Surface Science, 12, 109 (1968).

68. C. MATANO, Jap. J. Phys., 8, 109 (1933).

69. C. WAGNER, Acta Met., 17, 99 (1969).

70. JOE H. DOYLE, "Computer Programs to Determine Chemical Diffusivities Using the Boltzman-Matano Analysis," RFP 1544 UC-4 Chemistry TID 4500, 56 Ed. 1971.

ACKNOWLEDGMENTS

This study was supported through the Air Force Office of Scientific Research, Contract #F33615-68-C-1034 (properties of ceramic materials). Experimental work was performed for the most part in the Ames Laboratory, USAEC under an associate appointment.

The author wishes to thank both his major professor, Dr. Donald M. Roberts and Dr. Michael F. Berard for countless helpful discussions and useful suggestions throughout the course of this investigation. Appreciation is also expressed to Mr. C. D. Wirkus for conducting electron microprobe analysis of the diffusion anneals. The author also thanks Dr. Glenn Murphy and A. F. Voigt for their assistance. Several other individuals in the Ceramic Engineering Department of Iowa State University and the Ceramic Engineering Division of Ames Laboratory have made contributions during various phases of this study.

APPENDIX

Modifications of Fick's Laws

Starting with Fick's laws in their most general form,

$$J_i = -D_{ij}C_{,j} \qquad \text{Fick's first law} \qquad \text{(A-1)}$$

$$\dot{C} = (D_{ij}C_{,j})_{,j} \qquad \text{Fick's second law} \qquad \text{(A-2)}$$

and using the following well-known relations,

$$\mu_{,j} = \frac{kT}{C} C_{,j} \qquad \text{(A-3)}$$

and

$$B_{ij}kT = D_{ij} \qquad \text{(A-4)}$$

where

μ = chemical potential

B_{ij} = mobility

and all other symbols have their usual meanings one obtains the following equations for Fick's laws.

$$J_i = B_{ij}C\mu_{,j} \qquad \text{(A-5)}$$

$$\dot{C} = (B_{ij}C\mu_{,j})_{,j} \qquad \text{(A-6)}$$

Now the gradient of the chemical potential is seen to be the variable of interest.

Important cases do arise in which nonideal mixing occurs, so one proceeds to introduce activities into Fick's equations.

$$\mu = \mu^{\circ} + kT \log a \tag{A-7}$$

where

a = activity

Equations (A-5) and (A-6) now become

$$J_i = -B_{ij}\, kTC\, \frac{1}{a}\, a_{,j} \tag{A-8}$$

$$\dot{C} = [B_{ij} kT\, \frac{\partial \log a}{\partial \log C}\, C_{,j}]_{,j} \tag{A-9}$$

$$\text{i.e. } C = \frac{\partial C}{\partial \log C}$$

Then noting that

$$a = \gamma C \tag{A-10}$$

and

$$d \log C = d \log N$$

where

γ = activity coefficient

N = mole fraction

and using Equation (A-4), one obtains

$$J_i = -D_{ij}[1 + \frac{\partial \log \gamma}{\partial \log N}]C_{,j} \tag{A-11}$$

and

$$\dot{C} = ([D_{ij}(1 + \frac{\partial \log \gamma}{\partial \log N})]C_{,j})_{,j} \tag{A-12}$$